Freymuth, H., Ivko, B., Gill, J. B., Tamura, Y., & Elliott, T. (2016). Thorium isotope evidence for melting of the mafic oceanic crust beneath the Izu arc. *Geochimica et Cosmochimica Acta*, *186*, 49-70. https://doi.org/10.1016/j.gca.2016.04.034

Thorium isotope evidence for melting of the mafic oceanic crust beneath the Izu arc

Heye Freymuth[1], Ben Ivko[1], James B. Gill[2], Yoshihiko Tamura[3], Tim Elliott[1]

[1]*Bristol Isotope Group, School of Earth Sciences, University of Bristol, Wills Memorial Building, Queen's Road, Bristol BS8 1RJ, UK*

[2]*Department of Geology, University of California, 1156 High Street, Santa Cruz, California 95064, USA*

[3]*Institute for Research on Earth Evolution, Japan Agency for Marine-Earth Science and Technology, 3175-25 Showa-machi, Kanazawa-ku, Yokohama 23609991, Japan*

Abstract

We address the question of whether melting of the mafic oceanic crust occurs beneath ordinary volcanic arcs using constraints from U-Series ($^{238}U/^{232}Th$, $^{230}Th/^{232}Th$ and $^{226}Ra/^{230}Th$) measurements. Alteration of the top few hundred meters of the mafic crust leads to strong U enrichment. Via decay of ^{238}U to ^{230}Th, this results in elevated ($^{230}Th/^{232}Th$) ratios over time-scales of ~350 ka, where brackets indicate activity ratios. This process leads to the high ($^{230}Th/^{232}Th$), between 2.6-11.0 in the mafic altered oceanic crust (AOC) sampled at ODP Sites 801 and 1149 near the Izu-Bonin-Mariana arc. Th activity ratios in the Izu arc lavas range from ($^{230}Th/^{232}Th$) = 1.2-2.0. These values are substantially higher than those in bulk sediment subducting at the Izu trench and also extend to higher values than in mid-ocean ridge basalts or the Mariana arc. We show that the range in Th isotope ratios in the Izu arc lavas is consistent with the presence of a slab melt from a mixed source consisting of AOC and subducted sediments with an AOC mass fraction of up to approximately 80 wt.% in the component added to the arc lava source. The oceanic plate subducting at the Izu arc is comparatively cold which therefore indicates that temperatures high enough for fluid-saturated melting of the AOC are commonly achieved beneath volcanic arcs. The high ratio of AOC/sediments of the slab melt component suggested for the Izu arc lavas requires preferential melting of the AOC. This can be achieved when fluid-saturated melting of the slab is triggered by fluids derived from underlying subducted serpentinites. Dehydration of serpentinites and migration of the fluid derived into the overlying crust causes melting to start within the AOC. The absence of a significant sediment melt component suggests there was insufficient water to flux both AOC and overlying sediments.

1. Introduction

Subduction zones are the primary locations where material from the Earth's surface is recycled into the mantle. This material, collectively termed 'subducted slab', consists of the oceanic crust and the underlying lithospheric mantle. There is abundant evidence in the compositions of volcanic arc magmas for components derived from the subducting slab (e.g. Armstrong, 1968; Tatsumoto, 1969; Gill, 1981; Brown et al., 1982; White and Dupré, 1986; Plank and Langmuir, 1993). In particular, arc magmas are argued to contain components derived from subducted sediments that are thought to be transported into the mantle wedge as melts (e.g. Elliott et al., 1997; Hawkesworth et al., 1997; Johnson and Plank, 1999; Class et al., 2000). Early studies proposed that the underlying mafic altered oceanic crust (AOC) was the primary source of arc magma (Green and Ringwood, 1968). More recently, dehydration rather than melting of the AOC has been thought to provide fluids and fluid-mobile elements to a mantle source of arc magmas (e.g. Gill, 1981; Pearce, 1982; Tatsumi et al., 1986).

An exception to this scenario has been argued for the compositionally unusual adakites and some high-Mg andesites that are believed to include large mass fractions of melt of the AOC (e.g. Kay, 1978; Defant and Drummond, 1990; Furukawa and Tatsumi, 1999; Yogodzinski et al., 2001; Gómez-Tuena et al., 2007; Kimura et al., 2014). However, production of these magma types is related either to subduction of very young oceanic crust (Defant and Drummond, 1990; Peacock et al., 1994; Furukawa and Tatsumi, 1999) or to circumstances where the oceanic plate experiences unusual heating, e.g at slab edges or slab windows (Abratis and Wörner, 2001; Yogodzinski et al., 2001; König and Schuth, 2011). Yet interpretation of adakites or adakite-like magmas remains controversial and some attribute examples of these compositions to mid- or lower-crustal processes (e.g. Arculus et al., 1999; Garrison and Davidson, 2003; Chiaradia, 2009; Zellmer et al., 2012).

These geochemical inferences can be compared with experimental petrology and numerical, thermal models. Solidus temperatures for metabasalts and metasediments are similar under fluid-saturated conditions at sub-arc depth (e.g. Nichols et al., 1994; Schmidt et al., 2004). Thus, conditions favorable for melting of subducted sediments should also lead to melting of the AOC unless the thermal gradient through the slab is too great (Kelemen et al., 2003). Current thermal models produce pressure-temperature paths for the top of the AOC that reach or exceed conditions of H_2O saturated melting beneath most arcs (van Keken et al., 2011), demonstrating that melting of the AOC could be a common phenomenon in subduction zones if water is added to the system. While geochemical observations argue for melting of subducted sediments beneath volcanic arcs similar evidence for melting of the AOC is more controversial. Slab melts consisting of a mixture of AOC and subducted sediments have been suggested to contribute to the source of lavas erupted in the Izu backarc (Hochstaedter et al., 2001; Kimura et al., 2010; Tollstrup et al., 2010). A similar suggestion

has recently been made for arc front magmas from the western Aleutian arc (Kelemen et al., 2003; Yogodzinski et al., 2015) where a relatively hot slab is subducting (van Keken et al., 2011). It therefore appears that melting of the AOC within subduction zones may occur in at least some arc and backarc settings, but this has not been viewed as a process that occurs beneath ordinary volcanic arcs.

Detection of AOC melts in arc magmas is challenging because 1) key incompatible trace elements in melts of the hot, upper slab should generally be dominated by the sediment component and 2) alteration of the oceanic crust has minimal influence on some isotopic systems used as tracers for melt source compositions ($^{143}Nd/^{144}Nd$, $^{176}Hf/^{177}Hf$), often making AOC melts difficult to distinguish from melts of the sub-arc mantle. Other traditionally used radiogenic isotopes belong to distinctly fluid-mobile elements (Sr, Pb) and their budget is therefore not solely contributed by the slab-melt component. This makes such tracers less sensitive to the role of a slab-melt contribution. In addition, while melts of the eclogitic slab components should be distinctly depleted in heavy rare earth elements, these will be likely overprinted by contributions from the sub-arc mantle (Straub et al., 2013).

Here we propose the $^{230}Th/^{232}Th$ ratio as a novel tracer for an AOC melt component in arc magmas. ^{230}Th has a half-life of 75 ka and is produced by the decay of ^{238}U while ^{232}Th is a long-lived radioactive nuclide with a half-live of ~14 Ga. Processes that cause variations in the U/Th ratios lead to corresponding changes in $^{230}Th/^{232}Th$ over the course of ~350 ka (five times the half-live of ^{230}Th). The $^{230}Th/^{232}Th$ ratio is therefore a direct measure of the U/Th ratio at timescales longer than a few hundred thousand years. In mid-ocean-ridge basalts (MORB) the range in ($^{230}Th/^{232}Th$) (where brackets indicate activity ratios) is limited (Fig. 1) because of the homogeneity of upper mantle sources and the minor fractionation of two highly incompatible elements, such as Th from U, during the large degrees of sub-ridge melting. Arc lavas have a wider range in ($^{230}Th/^{232}Th$) that extends to both lower and higher values relative to MORB (Fig. 1). Low ratios of ($^{230}Th/^{232}Th$) in arc lavas have been attributed to the addition of pelagic clay to the arc magma source (e.g. Allègre and Condomines, 1982; Gill and Williams, 1990; McDermott and Hawkesworth, 1991). The reason for ($^{230}Th/^{232}Th$) ratios of some arc lavas higher than MORB has so far been less clear. Possible explanations for high ($^{230}Th/^{232}Th$) ratios include metasomatism of the arc magma mantle source followed by aging and ingrowth of ^{230}Th (Gill and Williams, 1990; Gill et al., 1993; Regelous et al., 1997; Turner et al., 1997; Turner et al., 1998), high and variable degrees of mantle depletion (e.g. Gill and Williams, 1990; Caulfield et al., 2012), addition of carbonate sediment to the arc magma source (Reagan et al., 1994), and derivation of Th from the AOC via a fluid component (McDermott and Hawkesworth, 1991).

In this contribution we explore the high ($^{230}Th/^{232}Th$) in the Izu arc and examine the possible role of

the AOC melts in their generation. Notably, alteration of the top few hundred meters of the mafic oceanic crust is associated with strong U enrichment (e.g. Aumento et al., 1976; MacDougall, 1977; Hart and Staudigel, 1982). This leads to high ($^{230}Th/^{232}Th$) ratios in the AOC, e.g. ($^{230}Th/^{232}Th$) = 7 in the super composite of the ODP Site 801 AOC super composite described in Kelley et al. (2003), assuming secular equilibrium. Even though Th concentrations in the AOC are typically more than an order of magnitude lower than in sediments, the ($^{230}Th/^{232}Th$) ratio in slab melts could be significantly affected by the addition of AOC melt components with such extreme values of this ratio. The Izu arc lavas, with a minimal sediment contribution inferred in their source (Taylor and Nesbitt, 1998), should therefore be particularly sensitive to Th addition from an AOC melt.

New U-Series as well as major, trace element and radiogenic Sr, Nd and Hf isotope data are presented here for lavas from five volcanoes of the Izu volcanic front and one volcano from the Izu backarc. The new Izu arc data are compared to data from the well-studied Mariana arc located at the southern end of the Izu-Bonin Mariana arc system (Fig. 2). Input parameters for the Izu and Mariana arc can be constrained unusually well from ODP Site 801 outboard the Mariana arc and ODP Site 1149 outboard the Izu arc (Fig. 2) both of which sampled the entire sediment section and part of the underlying mafic AOC (Lancelot et al., 1990; Plank et al., 2000). In general, Marina arc lavas seem to have a larger mass fraction of sediment in their mantle source than in Izu (e.g. Woodhead and Fraser, 1985; Woodhead et al., 1987; Woodhead, 1989; Elliott et al., 1997) and are thus a useful reference.

2. Materials and methods

2.1 Samples and sample preparation

Samples used in this study are from Oshima, Miyakejima, Hachichojima, Aogashima, Torishima from north to south along the volcanic front, and Niijima which is ~15 km behind the front in the north (Fig. 2). Eight samples are from historical eruptions and the rest are thought to be younger than than 10 ka based on their geological context (Table 1).This assessment was borne out by analysis of several samples of unknown age for $^{226}Ra/^{230}Th$ disequilibrium (see section 3). All the Torishima samples are the High-Zr type of Tamura et al. (2007). In addition to the arc lavas, 8 samples of volcaniclastic sediments from ODP sites 800, 801 and 802 were analysed for their Th isotope ratios.

Samples from Niijima, Hachijojima, and samples 1469, 1874, and 1983-2903 from Miyakejima were obtained as powders. Details on powder preparation procedures for these samples are reported by Kimura et al. (2010), Ishizuka et al. (2008), and Fukuda et al. (2008), respectively. Samples from

Oshima, Aogashima, Torishima, and samples MJ-12-02 and MJ-12-05 from Miyakejima were processed as follows. Rocks were sawn into slices approximately 1 cm wide and then gently abraded with a diamond polishing plate to remove possible contamination from the rock saw. The slices were then wrapped into several layers of paper and crushed by hand with a hammer. The rock chips were cleaned in MQ (18 MΩ) H_2O for several days. The solution was then tested for the presence of NaCl using $AgNO_3$, to assess any residual seawater in samples which included submarine flows and coastal lavas subjected to sea-spray. All samples were free of NaCl. The samples were then dried and rock chips of approx. <2 mm size were picked by hand to exclude chips with visible signs of alteration. Powders were then produced in an agate ball mill. Neither chips nor powders were acid leached.

2.2 Analytical methods

Major and trace elements were analysed by solution ICP-OES and ICP-MS respectively at the Lamont-Doherty Earth Observatory of Columbia University following the methods described in Kelley et al. (2003). Major element concentrations were determined on the same acid digests used for ICP-MS and silica content was calculated by sum deficit (see Wade et al., 2005 for details). Standards MAS1722, MAR, K1919 and W-2 were measured for trace elements together with the samples and used as calibration standards for ICP-ES analyses. Reference values for MAS1722 are reported in Cooper et al. (2010).

For radiogenic isotope analysis approximately 100 mg of powder was dissolved in a $HF/HNO_3/HCl$ mixture followed by complete dissolution of the samples in 6M HCl. Sr, Nd, and Hf were initially separated on chromatography columns using cationic AG50-X8 resin (Patchett and Tatsumoto, 1981). The Sr split was then further purified on Sr-spec resin and the Hf and Nd splits were purified on Ln-Spec resin following the methods of Münker et al. (2001) and Pin and Zalduegui (1997).

A ^{228}Ra spike was prepared by "milking" a ^{232}Th stock solution using cation exchange resin to separate Ra from Th. The cationic columns were repeated several times and followed by a final removal of remaining Th using TRU-spec resin, after which no ^{232}Th was detectable in the ^{228}Ra spike solution. For U-Th-Ra isotope analysis a $^{236}U/^{229}Th$ mixed spike (see details in Hoffmann et al., 2007) and the ^{228}Ra spike were added to 200-300 mg of sample which was then dissolved in a $HF/HCl/HClO_4$ mixture. This mixture was then dried down step-wise at 120 °C for 12 hours, 160°C for 12 hours and 200 °C for 12 hours, re-dissolved in $HCl/HClO_4$ and dried down in the same step-wise procedure followed by a final dissolution in HCl. Complete dissolution and thus sample- spike equilibration was ensured in the final stage. This dissolution method largely follows Yokoyama et al. (1999) who demonstrated that this step-wise drying and re-fluxing the sample in $HClO_4$ is efficient in removing insoluble fluorides. Initial separation of U, Th and Ra was achieved on TRU-

spec resin (Horwitz et al., 1993) with pre-filter resin in the bottom of the columns. The pre-filter-resin was also used in the bottom of the Sr-spec columns to remove organic material derived from the resin. The Th fraction was then further purified with AG1-X8 resin as suggested by Yokoyama et al. (2003). The Th purification is necessary to remove Zr which potentially creates interferences in the Th mass spectrum as $Zr_2O_3^+$ and can be present in the Th fraction derived from the TRU-spec columns.

Ra was separated with a procedure similar to those described by Chabaux et al. (1994) and Koornneef et al. (2010) but with generally smaller columns sizes. Resin volumes of the two cationic columns were 10 ml and 0.5 ml and the volume of Sr-Spec was 0.15 ml. The Sr-columns were repeated to improve the separation of Ba from Ra. In addition, HREE were removed after the cationic columns with 0.15 ml Ln-spec columns.

Purified U, Th and Ra fractions were dried down and re-dissolved in a mixture of conc. HNO_3 and H_2O_2 to decompose organic material that might have passed through the pre-filter resin and the frit material of the columns.

Sr isotope ratios were analysed on a Thermo Finnigan Triton in static mode. Results were corrected online for mass bias to $^{88}Sr/^{86}Sr = 8.375209$. The standard NIST SRM 987 was analysed at least four times per analytical session and samples were normalized to $^{87}Sr/^{86}Sr = 0.71025$ for NIST SRM 987. Measured values for NIST SRM 987 were $^{87}Sr/^{86}Sr = 0.710228 \pm 0.000026$ (N = 23). No significant isotopic differences were found for measurements of NIST SRM 987 that was processed through the column chemistry and unprocessed standard solution that was loaded directly onto the filaments.

Nd and Hf isotopes were measured on a Thermo Finnigan Neptune MC-ICP-MS. Nd isotope ratios were measured following the procedures of Vance and Thirlwall (2002) with an exponential mass bias correction to $^{146}Nd/^{144}Nd = 0.7219$ and normalization to either $^{143}Nd/^{144}Nd = 0.511853$ of La Jolla or $^{143}Nd/^{144}Nd = 0.512115$ of JNdi-1. Hf isotope ratios were measured as described by Rickli et al. (2013) with a normalization to $^{176}Hf/^{177}Hf = 0.282160$ of JMC 475. Results for rock standards analysed together with the samples were: JB-2: $^{143}Nd/^{144}Nd = 0.513106 \pm 3.7x10^{-6}$ (n=4), $^{87}Sr/^{86}Sr = 0.703672 \pm 2.6x10^{-5}$ (n=5), $^{176}Hf/^{177}Hf = 0.283252 \pm 3.0x10^{-6}$ (n=4) ; BCR-2: $^{143}Nd/^{144}Nd = 0.512636 \pm 2.1x10^{-6}$ (n=4), $^{87}Sr/^{86}Sr = 0.705007 \pm 2.2x10^{-5}$ (n=4), $^{176}Hf/^{177}Hf = 0.282869 \pm 3.0x10^{-6}$ (n=4); BHVO-2: $^{143}Nd/^{144}Nd = 0.512985 \pm 1.6x10^{-6}$ (n=2), $^{87}Sr/^{86}Sr = 0.703468 \pm 1.2x10^{-5}$ (n=2), $^{176}Hf/^{177}Hf = 0.283099 \pm 2.2x10^{-7}$ (n=2) (errors are 2σ standard deviations, n = number of analyses).

U and Th isotope ratios were measured on a Thermo Finnigan Neptune MC-ICP-MS in static mode in separate sequences. Mass bias corrections were made using sample-standard bracketing with NBL SRM-112a for U and the in-house standard 'Thosi' for Th. A feedback amplifier with a 10^{12} Ω

resistor was used for measurement of the ^{236}U and ^{229}Th beams on Faraday cups while ^{234}U and ^{230}Th were measured with a secondary electron multiplier (SEM) in the axial position. SEM non-linearity was corrected for as described by Hoffmann et al. (2005). Tailing of the ^{238}U and ^{232}Th beams was measured in the beginning and at the end of each analytical sequence at masses 233.4, 233.5, 233.6, 234.4, 234.5, 234.6, 235.4, 235.5, 235.6, 236.4, 236.5, 236.6 and 228.5, 229.4, 229.5, 229.6, 230.4, 230.5, 230.6, respectively, and corrections applied to ^{234}U, ^{230}Th and ^{229}Th using interpolations of exponential fits of abundance sensitivity against mass using these background measurements (see Hoffmann et al. 2007). The ^{236}U beam intensity was simultaneously corrected for ^{238}U tailing and ^{235}U hydride using $^{236}U/^{238}U$ ratios by using the on-peak baseline measured in a ^{236}U-free bracketing standard. Sufficient quantities of ^{236}U spike were used in samples to keep this correction to ~1 ‰. A retarding potential quadrupole (RPQ) lens was used for Th isotope measurements to reduce the magnitude of the tailing of ^{232}Th on ^{230}Th to typical values of 2×10^{-8} which was usually less then 1% of the signal intensity of ^{230}Th.

Ra isotope ratios were measured on a Thermo Finnigan TRITON by peak-jumping between ^{226}Ra and ^{228}Ra on the SEM. A correction for time varying count rates was made using the method described by Coakley et al. (2005). The $^{228}Ra/^{226}Ra$ of the spike was calibrated during each analytical session by measuring it in a similar way to the samples and the spike Ra concentration was calculated from measurements of spiked BCR-2 standards, assuming secular equilibrium for BCR-2 (Prytulak et al., 2008). Instrumental mass fractionation of $^{228}Ra/^{226}Ra$ was assumed to be negligible.

3. Results

Major and trace element data for the Izu arc lavas and reference materials are reported in Table 1 and Table 2. All samples analysed for this study are basalts or basaltic andesites with the exception of sample 881105-2 from Aogashima which is an andesite.

Fig. 3 shows a trace element variation diagram in which the Izu arc lavas are compared to the Mariana arc lavas. Heavy rare earth element (HREE) concentrations in the Izu and Mariana arcs are similar but the Izu volcanic front lavas are more depleted in the highly incompatible elements compared to the Mariana arc lavas. Magmas erupted in the Izu rear arc (Niijima) are generally more enriched in incompatible elements compared to the Izu volcanic front except for some fluid-mobile elements (see also Kimura et al., 2010; Tollstrup et al., 2010; Hochstaedter et al., 2000; Hochstaedter et al., 2001).

It has previously been shown that contrasting compositions of samples from different islands of the Izu arc do not show systematic variations in incompatible trace element ratios (Taylor and Nesbitt,

1998). Although this is also the case in our dataset, Ba and to a lesser extent Th, are most enriched in the two northernmost islands, Oshima and Miyakejima (Fig. 4). Fig. 5a shows the variation in Ba/Th vs. La/Sm in samples of the Izu arc compared with the Mariana arc. The Mariana arc lavas form a coherent trend from high Ba/Th and low La/Sm to low Ba/Th and high La/Sm that has previously been interpreted as a result of the near constant addition of a fluid derived from AOC (with high Ba/Th) to a depleted mantle source that is variably enriched by a sediment melt (with high La/Sm and low Ba/Th) (Elliott et al., 1997). Similar trends seem to exist within some of the Izu islands (Fig. 5a), but the inter-island variation in the Izu volcanic front is different with a large variations in Ba/Th over a limited rage of La/Sm. The two northernmost, volcanic front islands lie along the Mariana trend, but the others have lower La/Sm at a given Ba/Th. The two southernmost islands have the lowest Ba/Th of the arc front and backarc Niijima has the highest La/Sm.

Sr, Nd and Hf isotope ratios for Izu arc lavas and standards are reported in Table 3. Radiogenic Sr isotope ratios in the Izu arc lavas vary positively with Ba/Th (Fig. 5b), apart from Miyakejima samples that have anomalously unradiogenic Sr and Pb isotope ratios (Taylor and Nesbitt, 1998). Samples from Niijima have lower $^{87}Sr/^{86}Sr$ and $^{143}Nd/^{144}Nd$ than the volcanic front lavas. This is a general characteristic of the arc front to back-arc geochemical variation in the Izu arc (e.g. Hochstaedter et al., 2001; Ishizuka et al., 2003; Kimura et al., 2010; Tollstrup et al., 2010).

Inter-island differences in our Nd and Hf isotope measurements are subtle but clearly resolvable (Fig. 6). Some literature data for more differentiated rocks from on or near Miyakejima and Aogashima extend to lower $^{143}Nd/^{144}Nd$ at the same $^{176}Hf/^{177}Hf$ (Fig. 6). Most Izu arc lavas fall within the Nd-Hf isotope field of Shikoku Basin and Mariana Trough basalts (Fig. 6) in contrast to the Mariana arc which requires the addition of slab-derived sediment to the arc mantle sources (Tollstrup and Gill, 2005; Woodhead et al., 2012).

U-Series data for the Izu arc lavas are reported in Table 4. All samples analysed for ^{226}Ra concentrations are in ($^{226}Ra/^{230}Th$) disequilibrium (Fig. 7). This signifies recent Ra addition and indicates that in cases where age constraints are not available the eruptions occurred less than ~8000 years ago (five times the half live of ^{226}Ra). These samples were thus clearly not affected by significant post-eruptive ingrowth of ^{230}Th (with a half live of 75 ka) and we therefore interpret their ($^{230}Th/^{232}Th$) and ($^{238}U/^{230}Th$) ratios as initial values. The ($^{226}Ra/^{230}Th$) and ($^{238}U/^{230}Th$) ratios are within the range of previously reported data for volcanic arcs (see compilation in Turner et al., 2003) and as in most arcs there is no obvious correlation between Ra excess and U excess (Fig. 7). In addition, the Ra excesses in the Izu arc lavas are within the range of Ra excesses observed for MORB (see compilation in Lundstrom, 2003). Thus the possible influence of slab derived Ra addition and decay during transport cannot be readily distinguished from the effects of purely decompression melting processes in the upper mantle.

Intra-island variations in ($^{230}Th/^{232}Th$) and ($^{238}U/^{232}Th$) are generally small with each island forming a well defined cluster in a ($^{230}Th/^{232}Th$) vs. ($^{238}U/^{232}Th$) equiline diagram (Fig. 8). This suggests that the few samples with unconstrained eruptions ages are similar in age to the other samples and were not affected by significant post-eruptive ingrowth of ^{230}Th. Our U-Th isotope data for Mijakejima, Oshima and Niijima are similar to previously published data for these islands, eruptions, and in some cases same samples by Yokoyama et al. (2003) and Fukuda et al. (2008) (Fig. 8). In a detailed study of Miyakejima, Yokoyama et al. (2003) subdivided the recent eruptive history into four stages and showed that samples from stages 1 and 2 (>7000 years and 7000-4000 years BP, respectively) form two approximately horizontal trends in a ($^{230}Th/^{232}Th$) vs. ($^{238}U/^{232}Th$) equiline diagram whereas samples from the younger stages 3 and 4 (2500 years BP - 1154 AD and 1469-1983 AD, respectively) are affected by mixing between the stage 1 and 2 magma types and have intermediate ($^{230}Th/^{232}Th$). Our data for Miyakejima are from stages 3 and 4 and agree with those of Yokoyama et al. (2003) from the same stages.

Samples from Oshima and Niijima plot on the high and low ends in ($^{238}U/^{232}Th$) of the well-defined trend of the Mariana arc on an equiline diagram (Fig. 8). Samples from Miyakejima, Hachijojima, and Torishima have increasingly elevated ($^{230}Th/^{232}Th$) at near constant U-excesses of ~30 %. Samples from Aogashima have high ($^{230}Th/^{232}Th$) but modest U-excess of ~10%. The variation in ($^{230}Th/^{232}Th$) extends over a much larger range than previously recognized in Izu, being higher in the two southern islands than the northern three. Samples from Torishima have amongst the highest ($^{230}Th/^{232}Th$) of arc lavas worldwide (cf Fig.1).

Th isotope data for volcaniclastic sediments from ODP Sites 800, 801 and 802 also are presented in Table 4. It has been suggested that these sediments dominate the sediment component in the Mariana arc lavas (Tollstrup and Gill, 2005; Woodhead et al., 2012; Avanzinelli et al., 2012) and are therefore important input parameters for the Mariana arc. The volcaniclastic sediments have variable Th isotope ratios with ($^{230}Th/^{232}Th$) = 0.38-0.92 but the average 0.64 ± 0.21 (1SD) is similar to previous estimates for the bulk sediment at the Mariana arc: 0.56 (Elliott et al., 1997), 0.64 (Plank and Langmuir, 1998), assuming secular equilibrium. Moreover, all of our measured ratios are lower than Avanzinelli et al.'s (2012) estimate for volcaniclastic sediments subducting at the Mariana arc based on gamma-ray logs (($^{230}Th/^{232}Th$)=0.95).

4. Discussion

4.1 Th isotope compositions of subducted sediments and AOC

Potential sources for the Th in Izu arc lavas are the sub-arc mantle, subducted sediments, and the

AOC. Constraining their relative importance requires knowledge of their Th contents and isotopic compositions. Thorium isotope ratios of the sediments and the AOC from ODP Sites 801 and 1149, off-board Mariana and Izu arcs respectively, are shown in Fig. 9. The sediment compositions at the two sites are described in detail in Plank et al. (2000). The sediment piles at both sites are 400-500 m thick and are subducted completely without forming accretionary wedges. Both sites contain basal sections of radiolarite cherts and Th-rich pelagic clays that are more dominant in ODP Site 1149. The upper sediments at Site 1149 contain dispersed loess from China and ash from Japan with high Th/U (Scudder et al., 2009). ODP Site 801 contains an additional ~180 m thick sequence of mid-Cretaceous OIB volcaniclastics that is absent from ODP Site 1149. Despite these differences, the bulk sediment compositions from the two sites have remarkably similar U/Th ratios and, therefore, Th isotope composition assuming secular equilibrium, namely (^{230}Th/^{232}Th) = 0.65 for ODP Site 1149 (Plank et al., 2007) and 0.64 for ODP Site 801 (Plank and Langmuir, 1998). These values are lower than observed in 2/3 of MORB (Fig. 9a, b).

The well documented addition of U to the upper mafic crust during alteration has an extreme influence on the (^{230}Th/^{232}Th), producing Th isotope ratios in the AOC at ODP Sites 801 and 1149 that are higher than in MORB (Fig. 9c, d) with average (^{230}Th/^{232}Th) = 7.01 (ODP Site 801) and 2.63 (ODP Site 1149). A different alteration mineralogy has been described for the AOC at the two sites (Plank et al., 2000) and might account for their different (^{230}Th/^{232}Th) ratios. However, it is unclear whether the limited sampling interval at Site 1149 is representative of the AOC. Indeed, neither site is deep enough to allow us to constrain the full depth to which U enrichment occurs. Data for deeper sections of the oceanic crust are rare due to the small number of drill holes that penetrate more than a few hundred meters into the mafic oceanic crust. At DSDP/ODP Hole 504B in the East Pacific, U enrichment via alteration extends to about 800 m (Bach et al., 2003; see also compilation of U concentrations in several DSPD/ODP cores in Dunk et al., 2002). Below this depth, U enrichment is less marked and U/Th ratios approach those of unaltered MORB.

4.2 Controls on (^{230}Th/^{232}Th) in the Izu arc

U excesses in volcanic arc magmas are generally interpreted to result from recent U addition by fluids derived from subducted slabs (Gill, 1981; Newman et al., 1984; Condomines et al., 1988; Gill and Williams, 1990). Experimental mineral/fluid partition coefficients suggest that Th is also slightly mobile at pressures and temperatures relevant for subduction zones (see compilation in Turner et al. (2003)). Turner et al. (2003) thus showed that fluids in equilibrium with eclogites should have high but not infinite U excesses of 70 - 800%. Positive correlations between (^{238}U/^{232}Th) and (^{230}Th/^{232}Th) within genetically related samples such as in the Mariana arc (Fig. 8)

require the additional presence of a component with ($^{238}U/^{232}Th$) lower than in the fluids. The low ($^{238}U/^{232}Th$) component in the Mariana arc must also have a Th excess (Fig. 8) and has previously been interpreted as a sediment melt (Elliott et al., 1997; Avanzinelli et al., 2012). We refer to the low ($^{238}U/^{232}Th$) component more generally as a 'melt' component, given the discussion below which proposes it comprises melt from both AOC and sediment.

Bulk sediments subducted at the Izu and Mariana arcs are too low in ($^{230}Th/^{232}Th$) to constitute the melt component in either arc (Fig. 8). It has been argued that the sediment melt component in the Mariana arc is dominated by the volcaniclastic sediments of ocean island basalt affinity (Tollstrup and Gill, 2005; Woodhead et al., 2012; Avanzinelli et al., 2012). Averaged gamma log data suggested that these volcaniclastics have higher U/Th and hence ($^{230}Th/^{232}Th$) than the average sediment at ODP Site 801, making them a suitable melt end-member in the Mariana arc (Avanzinelli et al., 2012). Yet our new data for volcaniclastic sediments (Table 4) are within the range of ($^{230}Th/^{232}Th$) of previous estimates for the average sediments subducting at the Mariana arc. Thus, invoking a dominant volcaniclastic sedimentary contribution does not provide a ready explanation for the high ($^{230}Th/^{232}Th$) required for the melt component in the Mariana arc, even if this does help account for other geochemical observations (Avanzinelli et al., 2012). An increase in the ($^{230}Th/^{232}Th$) ratio of the sedimentary component could be achieved if sediment melting produces U excess followed by ingrowth of ^{230}Th in the sediment-enriched mantle wedge over a time-scale of >350.000 years (Elliott et al., 1997). However, such a process is unlikely to explain the even higher and variable ($^{230}Th/^{232}Th$) melt component required by most of the Izu arc lavas (Fig. 10a), especially when the limited potential for the presence of sediment melts in the Izu arc lavas is considered (Fig. 6). Addition of a 'pure' sediment melt is thus unlikely to generate the high ($^{230}Th/^{232}Th$) melt component in the Izu arc lavas.

Early release of fluids into the mantle wedge beneath the forearc could also produce high ($^{230}Th/^{232}Th$) ratios in the mantle wedge over time-scales of >350.000 years if the fluids carry substantial amounts of U (e.g. Condomines et al., 1988; Gill et al., 1993; Elliott et al., 1997; Regelous et al., 1997). Serpentinized peridotites from the Mariana forearc are enriched in some fluid-mobile elements but not U (Savov et al., 2005; Savov et al., 2007) which indicates that transport of U from the slab into the fore-arc mantle is insignificant. This is supported by experiments on AOC samples from ODP Site 1256 that were conducted at pressures of 0.4-0.7 GPa and show very low fluid/solid partition coefficients for U ($D^{fluid/rock} = 5.8x10^{-5} – 1.1x10^{-4}$) (Mutter et al., 2014). Another argument against such a model comes from the Th enrichment in arc lavas relative to MORB. While U addition to the mantle wedge would lead to ingrowth of ^{230}Th, it would not affect the Th concentration which is dominated by ^{232}Th. ($^{230}Th/^{232}Th$ ratios in the mantle are usually below 10^{-4}). Yet, the Izu arc lavas are enriched in Th over the similarly incompatible

element Nb when compared to MORB (Fig. 3, 10b). They therefore require Th to be dominantly derived from the subducted slab. Thus, the slab-derived Th in Izu must have uncommonly high ($^{230}Th/^{232}Th$) ratios.

Mariana arc lavas can be explained by the addition of two different slab components, one with high U/Th and excess-U that is thought to be a fluid, and another with lower U/Th, excess-Th, and higher Th contents that is thought to be a melt (e.g. Elliott et al., 1997). If the same model applies to Izu, then the difference between Izu and Marianas islands in an equiline diagram can be explained by the addition of the same fluid but a melt with variable U/Th and ($^{230}Th/^{232}Th$) (Fig. 10). Despite lower Th concentrations in the AOC than the sediments (by about a factor of 20), AOC can have substantial influence on the Th isotope ratios of mixed slab melts. This is illustrated in Fig. 11. The figure shows that a mixed sediment + AOC slab melt produces Th isotope ratios higher than in MORB and within the range of the Izu arc lavas if the fraction of AOC in the slab melt is in the range of about 60-90 wt.%. Such proportions are consistent with the estimates based on other isotopes for Izu backarc lavas (Hochstaedter et al., 2001; Kimura et al., 2010; Tollstrup et al., 2010). Changes in the AOC/sediment ratio and/or in the degree of alteration of the AOC have large effects on the ($^{230}Th/^{232}Th$) of the slab melt component when the AOC contribution is significant. Such variability can thus explain the range of ($^{230}Th/^{232}Th$) in the Izu arc lavas (Fig. 10, 11).

Quantitative models for the U and Th concentrations, U-Series disequilibria and radiogenic Hf and Nd isotope ratios produced by slab fluids and slab melts are shown in Fig. 10 and described in Table 5. The composition of AOC in these models is from ODP Site 801 because it sampled a more extensive section of the oceanic crust that is likely to be more representative of the crust subducted at the Izu arc than the small section of AOC sampled at ODP Site 1149. The fraction of AOC in the slab melts and fluids would be even higher if ODP Site 1149 was used instead, due to its lower average ($^{230}Th/^{232}Th$) (Fig. 9).

The Nb/Th and ($^{230}Th/^{232}Th$) ratios in the Izu arc lavas can be reproduced by slab melts with ~ 60-90 wt.% AOC (Fig. 10b). Th from the mantle wedge (represented by MORB in Fig. 10b) likely contributes additional Th to the erupted arc lavas but this contribution must be minor in the Izu arc lavas given the systematics of Fig 10b. We therefore model the U-Series disequilibia of the Izu lavas as a three component system of AOC melt, sediment melt, and a fluid derived from altered mafic crust (Fig. 10a, b). The non-systematic variation within the Izu arc (with the exception of a N-S increase in ($^{230}Th/^{232}Th$)) (Fig. 8, 10a) indicates that all three parameters vary independently.

The slab melt has a small Th excess using the D's in Table 5 (Fig. 10a). The U excess in the Izu arc lavas therefore requires the addition of a high U/Th slab fluid. We envisage the fluids to be derived from dehydration of subducted serpentine at the base of the crustal section, which pass through the slab and interact with mafic crust that has experienced variable degrees of alteration. This is

represented in Fig 10a as mixing between a fluid derived from unaltered MORB and a fluid derived from AOC. We argue below that the trace element budget of the fluid is likely dominated by the unaltered mafic crust and therefore we use a fluid end-member derived from 85 % unaltered MORB and 15 % AOC to illustrate the effect of fluid addition on the U-Series disequilibria in Fig. 10a. Using this fluid composition, the fraction of slab fluid in the total slab component is ~20-75 wt.%. A fluid derived from a more altered MORB source (as suggested e.g. for magmas from the Manus Basin by Beier et al., 2010) would influence the slab melt/slab fluid mixing proportions but would have only minor effect on the AOC/sediment ratio in the slab melt component (Fig. 10a).

Unlike for Th, the sub-arc mantle is significant contributor to the Hf and Nd budgets of the Izu arc lavas and hence their isotope ratios (Fig. 10 c). Indeed, we argue that the Hf and Nd isotopic variability in the Izu arc samples primarily mimicks the range seen in the basalts from the Shikoku Basin and Mariana Trough that are minimally affected by subduction (Fig 6), and should be representative of sub-arc mantle prior to the addition of slab components. In Fig 10 c we show the influence on Hf and Nd isotope ratios of adding slab melts with the same AOC/sediment ratios as used to model Th isotope ratios (Fig. 10a, b). Among the Izu arc lavas only samples from Oshima and Niijima are significantly offset from mantle values in Nd and Hf isotope ratios (Fig. 6). To reproduce their data we require compositional variablity in the mantle, as illustrated in Fig. 10c where a highly depleted mantle composition is needed for Oshima and a less depleted mantle is needed for Niijima. The fractions of slab melts added to their mantle sources in these models are ca. 5 wt.% which is in line with previous suggestions of <2-6 wt.% for the Izu arc and back-arc (Chauvel et al., 2009; Tollstrup et al., 2010). However, the slab melt fractions and AOC/sediment melt ratios of the slab melts in Fig. 10c depend on the composition of the local mantle beneath each island which is currently poorly constrained. In addition, minor Nd contributions by fluids as discussed for the Mariana arc by Woodhead et al. (2012) could affect the amount of slab melt required to be added to the mantle.

4.3 Model for generating mixed AOC + sediment slab components in arc magmas

The large range in ($^{230}Th/^{232}Th$) of the Izu lavas is in keeping with other high ($^{230}Th/^{232}Th$) arcs such as New Britain and Tonga/Kermadec (Fig. 8) but notably in contrast with the adjacent Marianas arc. The well-defined trend in ($^{230}Th/^{232}Th$) vs. ($^{238}U/^{232}Th$) in the Mariana arc (Fig. 1, 8) demonstrates that a melt composition with approximately constant ($^{230}Th/^{232}Th$) is required throughout the Mariana arc, except for Alamagan, despite the variable mass fraction of enriched (sediment-like) components in the Mariana arc mantle sources (Elliott et al., 1997). Fig. 11 qualitatively accounts for these differences. Mixed slab melts with low AOC fractions (the left part

of Fig. 11) will have very little variation in absolute Th isotope ratios over large ranges of AOC/sediment mixing ratios. Minor changes in the AOC/sediment ratio of the slab melt will only have significant effects on ($^{230}Th/^{232}Th$) if the slab melt has a substantial fraction of AOC (the right part of Fig. 11). This suggests that the AOC/sediment ratio in the slab melt component of the Mariana and other oceanic arcs could potentially vary substantially but, as long as slab melts are >60% from sediment, their Th isotope compositions will be buffered by the sediments. As discussed above, the melt component in the Mariana arc lavas has higher ($^{230}Th/^{232}Th$) than the subducted sediments, requiring some melting of AOC even though less than in the Izu arc.

Recent models have suggested that the slab melt components in the western Aleutian arc (Yogodzinski et al., 2015) and the Izu backarc (Hochstaedter et al., 2001; Kimura et al., 2010; Tollstrup et al., 2010) are derived from AOC-rich sources. In fact, the Pb and Hf isotope arguments in these papers suggest 90-95% AOC in the source of the Izu backarc slab component. The Th isotope ratios show that the Izu volcanic front also contains a dominant AOC component, although with lower AOC/sediment ratios. Together, these examples indicate that melting of the AOC is common beneath modern arcs and that the component in arc magmas previously identified as a "sediment melt" is usually a melt of both sediment and AOC.

Melting of the AOC has previously been suggested to occur in subduction zones with atypically hot slabs (e.g. Cai et al., 2014; Kimura et al., 2014; Yogodzinski et al., 2015), implying that abnormally high temperatures are required to allow slab melting to extend into the AOC. Although the Izu arc has intermediate to low thermal parameters and slab-top temperatures (Syracuse et al., 2010; van Keken et al., 2011) we invoke melting of parts of the AOC in addition to the subducted sediments. Solidus temperatures for metabasalts and metasediments are similar under fluid-saturated conditions at sub-arc depth (Nichols et al., 1994; Schmidt and Poli, 1998; Johnson and Plank, 1999; Schmidt et al., 2004). Thus, if melting of the slab were controlled solely by pressure and temperature, the entire sediment column would be required to melt before the onset of melting in the AOC. Given a sediment thickness of 400 m, the need for > 80 wt. % AOC in the slab melt in some Izu arc lavas (Fig. 10, 12) requires melting of >1600 m of AOC. As discussed in 4.1, the depth to which the mafic oceanic crust is highly altered and enriched in U/Th (and thus has high ($^{230}Th/^{232}Th$)) is likely to be only about 800 m. Therefore, preferential melting of the AOC is required to generate slab melts with sufficiently high AOC/sediment ratios.

The flux of slab-derived components into the Izu arc magma sources can be further evaluated using mass balance calculations. The detection of ^{10}Be in some volcanic arc magmas has provided important evidence for the presence of sediment-derived components in their sources (e.g. Brown et al., 1982; Tera et al., 1986; Morris et al., 1990). Using the parameters in Table 6, we calculate that approximately 4.4 % of the (decay-corrected) subducted sedimentary ^{10}Be is recycled in Izu arc

490 magmas. A slightly larger fraction of 7.3 % of the Th transported to sub-arc depth in subducted
491 sediments and the AOC is recycled into the Izu arc lavas. 78-93 % of this Th is derived from
492 subducted sediments and 7-22 % from the AOC. This corresponds to 6.3-7.5 % of the sediment-
493 hosted Th and 5.5-17 % of AOC-hosted Th being removed from the slab and transported into the
494 Izu arc magma sources. The comparatively low mobilization of ^{10}Be and Th from sediments is in
495 line with earlier interpretations of low amounts of sediment-derived components in the Izu arc
496 magma sources which could be related to some sediments being scraped off beneath the fore-arc or
497 to limited interaction between the slab-derived fluids and sediments.
498 The above calculations show that, at least for the Izu arc lavas with high (^{230}Th/^{232}Th) ratios, the
499 fraction of Th mobilized from the AOC is higher than the fraction of Th mobilized from the
500 sediments, thus supporting the view that the AOC needs to melt preferentially compared to the
501 sediments. In order to explain this inference we propose that the amount of available H_2O is the
502 limiting factor controlling melting of the slab. At sub-arc depth the subducting oceanic crust is
503 mostly dehydrated (van Keken et al., 2011) so that external water is required for water-saturation.
504 Dehydration of subducted serpentinites has been proposed to be a major contributor to the fluid
505 budget in subduction zones (Ulmer and Trommsdorff, 1995; Peacock, 2001; Spandler et al., 2011;
506 van Keken et al., 2011). Serpentine dehydration occurs at pressures corresponding to ~80->150 km
507 depth and can therefore lead to fluid-saturation in otherwise mostly dehydrated crust. Importantly,
508 the water from the serpentinites enters the upper oceanic crust from below, encountering the AOC
509 before the overlying sediments. Water-saturated melting of the slab should therefore start in the
510 AOC rather than in the sediments. Water-saturated melting of the AOC leads to the formation of a
511 hydrous melt and thus consumes H_2O. The amount of available H_2O from serpentinites will
512 therefore control whether melting will also extend into the sediment layer. In systems with little
513 available H_2O, water-saturation could be mostly or completely restricted to the AOC.
514 This scenario requires that the amount of fluid released from serpentinites be highly variable
515 between and even within volcanic arcs in order to produce a range from AOC-dominated to
516 sediment-dominated slab melt sources. Fluid release from serpentinites underlying the oceanic crust
517 is controlled by the breakdown of hydrous phases which in turn depends on pressure and
518 temperature conditions. Dehydration of serpentinites primarily occurs via the breakdown of
519 antigorite (Ulmer and Trommsdorff, 1995) and is completed by ~115 km depth in hot subduction
520 zones (van Keken et al., 2011). In cold subduction zones the stability field of serpentine partially
521 overlaps the stability field of the hydro-magnesian phase A (Thompson, 1992; Ulmer and
522 Trommsdorff, 1995; Schmidt and Poli, 1998). The slab dehydration models of van Keken et al.
523 (2011) suggest that in the coldest subduction zones the overlap in the stability fields of serpentine
524 and phase A largely prevents the full dehydration of serpentinites. The availability of fluids from

serpentinites is therefore highly dependent on the P, T, t paths of the slab. The intermediate to low temperatures in the slab beneath the Izu arc might lead to overlap of the stability fields of serpentine and phase A and thus lead to a limited fluid-release beneath the arc that is enough to cause melting of the AOC but not the overlying sediments. Conversely, more fluid derived from serpentinites can be expected to be available in hotter subduction zones and lead to more sediment melting. In general, the latter should lead to lower ($^{230}Th/^{232}Th$) and could explain the low Th isotope ratios in Sunda and parts of the Lesser Antilles (Fig. 1). However, variations in the Th isotope compositions of local sediments, the overall amount of water subducted in serpentine, and the degree of alteration of the AOC all have major impacts on the ($^{230}Th/^{232}Th$) ratios of the arc lavas, thus limiting the potential of Th isotope ratios as a temperature indicator. The apparent north to south decrease in fluid addition and sediment melting at the Izu volcanic front might indicate southward decrease in serpentinite formation at the outer arc high east of the Izu Trench, or decreased fracture flow of fluids, either of which could localize water-saturated melting deeper in the subducting crust.

Fluids derived from dehydrating serpentinites traverse several kilometers of the deeper mafic oceanic crust which allows for a substantial contribution of less altered or unaltered oceanic crust to the fluid trace element budget, as suggested for the Mariana arc by Avanzinelli et al. (2012) and Freymuth et al. (2015). The trace element signature of arc lavas therefore derives from fluids that dominantly sample the deeper, unaltered oceanic crust, plus a slab melt generated from both AOC + sediment nearer the top of the oceanic crust. The Th isotope composition of the slab fluid in Fig. 10 requires a relatively unaltered source for Th and is therefore consistent with this model. The fluid and melt components in arc magmas can vary independently (Elliott et al., 1997) but may leave the slab as a single hydrous slab component that is added to the mantle source of arc magmas.

5. Conclusions

Exceptionally high ($^{230}Th/^{232}Th$) ratios generated in the oceanic crust as a consequence of U addition during alteration make Th isotope ratios a diagnostic tool for the detection of AOC melt components in arc magmas. Variable ($^{230}Th/^{232}Th$) ratios in volcanic front magmas from the Izu arc are consistent with the addition of a mixed sediment + AOC slab melt to the sub-arc mantle. Model calculations show that the fraction of AOC in the mixed slab melt component present in some Izu volcanic front magmas exceeds ~80 wt.% which is consistent with earlier suggestions for magmas from the Izu backarc.

The formation of slab melts with high AOC/sediment ratios requires preferential melting of the AOC compared to the overlying sediments. This can be achieved if the extent of slab melting is controlled by the availability of fluids from dehydrating serpentinites underneath the mafic crust.

Serpentinite dehydration occurs when subducted slabs approximately reach sub-arc depth. Fluids released from serpentinites encounter the AOC before the sediments. Slab melting should therefore start in the AOC if temperatures are high enough for melting to occur. The availability of fluids will then control whether the fluid-saturated conditions required for melting are also achieved in the sediment section of the subducted slab. In subduction zones where relatively cold slabs are subducting, such as the Izu arc, the amount of H_2O released from serpentinites is limited by the overlap of the stability fields of serpentine and the hydromagnesian phase A which prevents complete dehydration. This is not the case for hotter slabs in which complete dehydration of serpentinites occurs and consequently slab melts with lower AOC/sediment ratios can be expected.

Figure captions

Fig 1: ($^{230}Th/^{232}Th$) vs. ($^{238}U/^{232}Th$) equiline diagram with compiled U-Th isotope data for MORB and oceanic island arcs. Data for MORB are from PetBD (http://www.earthchem.org/petdb). Data for arc lavas are from Georoc (http://georoc.mpch-mainz.gwdg.de/georoc/) and Avanzinelli et al. (2012). Only samples for which ($^{234}U/^{238}U$) ratios were reported are plotted and data for samples with ($^{234}U/^{238}U$) >1.005 or <0.995 were considered altered and are excluded, except for those of Cunningham et al. (2012) where data appear systematically offset to ($^{234}U/^{238}U$) <1. Samples with SiO_2 >60 wt. % were also excluded to avoid those with possible fractionation of U/Th ratios caused by differentiation. Only subaerial arc lava samples were plotted due to the potential of U and Th contamination by seawater. One sample from the New Britain arc plots off- scale (with ($^{238}U/^{232}Th$) = 3.30, ($^{230}Th/^{232}Th$) = 2.85).

Fig. 2: Map of the Izu arc with sample locations. Basemap is from GeoMapApp (http://www.geomapapp.org).

Fig. 3: Relative incompatible element abundances of Izu arc lavas. Representative samples with MgO = 4.0-5.0 wt % are shown for each island (Oshima: 1986A-1, Niijima: NJ-2, Miyakejima: MJ-12-02, Hachijojima: 03103009, Torishima: 24, Aogashima: T87071906). The range in trace element concentrations in Mariana arc front lavas, as represented by endmember samples from Guguan (GUG9) and Uracas (URA6), is shown by the gray area. Mariana arc data are from Elliott et al. (1997). Trace element abundances are normalized to primitive mantle values of McDonough and Sun (1995).

Fig. 4: Trace element abundances in Izu arc lavas relative to SiO_2: a) Th, b) U, c) Ba, d) Nd. Large symbols are data from this study (Table 1, 2), small symbols are from Georoc (http://georoc.mpch-mainz.gwdg.de/georoc/).

Fig. 5: Izu arc lava variations in a) Ba/Th vs. La/Sm, b) Ba/Th vs. $^{87}Sr/^{86}Sr$. Symbols are the same as in Fig. 1. Large symbols are from this study, small symbols are previously published data (http://georoc.mpch-mainz.gwdg.de/georoc/). Data for the Mariana arc are shown for reference (Elliott et al., 1997). 'MORB' is the average and standard deviation of MORB from Jenner and O'Neill (2012). 'AOC fluid' and 'sediment melt' indicate the addition of AOC-derived fluids and sediment melts to the arc magma sources as suggested by Elliott et al. (1997).

Fig. 6: Hf and Nd isotope ratios in Izu arc lavas. Symbols are the same as in Fig. 1. Data plotted with large symbols are from this study, data plotted with small symbols are from Pearce et al. (1999), Tollstrup et al. (2010) and Kimura et al. (2010). A normalization to our values for the JB-2 standard has been applied to the Hf and Nd isotope ratios of Kimura et al. (2010) ($^{176}Hf/^{177}Hf$ = 0.283282 vs. 0.283252 and $^{143}Nd/^{144}Nd$ = 0.513076 vs. 0.513106, respectively). The Izu arc samples are compared to data for the Mariana arc volcanic front (Woodhead, 1989; Woodhead et al., 2001). The composition of the sub-arc mantle (blue shaded area) is estimated based on data for the Mariana backarc which were filtered to exclude samples influenced by subduction components (Woodhead et al., 2012) and the Shikoku backarc basin (Straub et al., 2010; Tollstrup et al., 2010). Errors bars in the top left corner indicate representative 2σ standard errors for data reported in this study.

Fig. 7: $(^{226}Ra/^{230}Th)_{initial}$ vs. $(^{230}Th/^{232}Th)$ for Izu arc samples. Symbols are the same as in Fig. 2. Data from this study are shown in large symbols. Data from Yokoyama et al. (2003) are shown in small symbols. Samples from Niijima, Hachijojima, and sample T87071906 from Aogashima have unconstrained eruption ages and their $(^{226}Ra/^{230}Th)$ ratios are therefore minimum values.

Fig. 8: $(^{230}Th/^{232}Th)$ vs. $(^{238}U/^{232}Th)$ equiline diagram with data from this study (large symbols) and previously published data (small symbols, data from Yokoyama et al. (2003) and Fukuda et al. (2008)). Symbols are the same as in Fig. 1 and Fig. 4. The 1:1 equiline is shown as solid black line. Dotted lines indicate 15 % fractions of U depletion or excess. SED 801 / 1149 are average compositions of the sediments from ODP Sites 801 and 1149, assuming secular equilibrium (see Fig. 9).

Fig. 9: Model Th isotope compositions in sediments and the AOC from ODP Sites 801 and 1149. Except for two volcaniclastic sediment samples from this study (Table 4), Th isotope ratios were calculated from U/Th ratios assuming secular equilibrium. Small symbols represent individual samples. Large symbols are average compositions for lithologic units (sediments) and stratigraphic sections (composite samples of AOC at ODP Site 801 and average of the AOC sampled at ODP Site 1149). The grey bars indicate the average Th isotope ratio and standard deviation of MORB (Jenner and O'Neill, 2012), assuming secular equilibrium. Dashed lines show average Th isotope values for sediments and AOC. Sources for individual data are: ODP Site 801 sediments: Karl et al. (1992), Plank et al. (1998), Table 4; ODP Site 1149 sediments: Plank et al. (2007); ODP Site 801 AOC: Kelley et al. (2003); ODP Site 1149 AOC: Kelley et al. (2003). Sources for average data are: ODP Site 801 sediments: Plank et al. (1998), ODP Site 1149 sediments: Plank et al. (2007), ODP

639 Site 801 AOC: Kelley et al. (2003) (composite samples), ODP Site 1149: weighted average from
640 Kelley et al. (2003).
641
642 Fig. 10: Models for the U-Th and Hf-Nd isotope composition of Izu arc lavas. The slab melts and
643 slab fluids are calculated using the parameters in Table 5 with melt and fluid fractions F = 0.1. a)
644 equiline diagram. Percentages in red next to the slab melt mixing line indicate the mass fraction of
645 AOC in the slab melt. The total slab component (fluid + sediment) is shown as a mixture between
646 two different slab melts (with 50 % and 90 % AOC, respectively) and a single slab fluid derived
647 from 85 % unaltered MORB and 15 % AOC. Percentages in black indicate the mass fraction of slab
648 fluid in the total slab component. b) (^{230}Th/^{232}Th) vs. Nb/Th. 'MORB' is the average and standard
649 deviation from Jenner and O'Neill (2012). Errors for Nb/Th and (^{230}Th/^{232}Th) ratios in the Izu arc
650 lavas are smaller than the symbol sizes. c) ^{176}Hf/^{177}Hf vs ^{143}Nd/^{144}Nd. Red and green curves show
651 mixing between slab melts (with 50 % and 90 % AOC, respectively, as in a) and b)) and two
652 different mantle melts that were chosen to be suitable for Oshima and Niijima, respectively. The
653 blue shaded area highlights potential mantle compositions and is the same as in Fig. 6. Percentages
654 in black indicate the fraction of slab melt in the slab-melt – MORB mixture.
655
656 Fig. 11: Mixing models for Th isotope ratios in slab melts. The average compositions of sediments
657 and the AOC from ODP Sites 801 and 1149 have been used as mixing end-members (see Fig. 9).
658 The grey bar indicates the range of Th isotope ratios in MORB (Fig. 1, with the exception of one
659 sample with (^{230}Th/^{232}Th) = 0.84).
660
661
662
663 **References**
664

Abratis M. and Wörner G. (2001) Ridge collision, slab-window formation, and the flux of Pacific asthenosphere into the Caribbean realm. *Geology* **29**, 127–130.

Allegre C. J. and Condomines M. (1982) Basalt genesis and mantle structure studied through Th-isotopic geochemistry. *Nature* **299**, 21–24.

Arculus R. J., Lapierre H. and Jaillard E. (1999) Geochemical window into subduction and accretion processes: Raspas metamorphic complex, Ecuador. *Geology* **27**, 547–550.

Armstrong R. L. (1968) A model for the evolution of strontium and lead isotopes in a dynamic Earth. *Rev*. *Geophys*. **6**, 175–199.

Aumento F., Mitchell W. S. and Fratta M. (1976) Interaction between seawater and oceanic layer two as a function of time and depth, 1. Field evidence. *Can Miner*. **14**, 269–290.

Avanzinelli R., Prytulak J., Skora S., Heumann A., G. K. and T. Elliott (2012) Combined 238U–230Th and 235U–231Pa constraints on the transport of slab-derived material beneath the Mariana Islands. *Geochim. Cosmochim. Acta* **92**, 308 – 328.

Avanzinelli R., Prytulak J., Skora S., Heumann A., Koetsier G. and Elliott T. (2012) Combined 238U–230Th and 235U–231Pa constraints on the transport of slab-derived material beneath the Mariana Islands. *Geochim. Cosmochim. Acta* **92**, 308–328.

Bach W., Peucker-Ehrenbrink B., Hart S. R. and Blusztajn J. S. (2003) Geochemistry of hydrothermally altered oceanic crust: DSDP/ODP Hole 504B – Implications for seawater-crust exchange budgets and Sr- and Pb-isotopic evolution of the mantle. *Geochem. Geophys. Geosystems* **4**, n/a–n/a.

Beier C., Turner S. P., Sinton J. M. and Gill J. B. (2010) Influence of subducted components on back-arc melting dynamics in the Manus Basin. *Geochem Geophys Geosyst* **11**, Q0AC03–.

Bird P. (2003) An updated digital model of plate boundaries. *Geochem Geophys Geosyst* **4**, 1027–.

Brown L., Klein J., Middleton R., Sacks I. S. and Tera F. (1982) 10Be in island-arc volcanoes and implications for subduction. *Nature* **299**, 718–720.

Cai Y., LaGatta A., Goldstein S. L., Langmuir C. H., Gómez-Tuena A., Martín-del Pozzo A. L. and Carrasco-Núñez G. (2014) Hafnium isotope evidence for slab melt contributions in the Central Mexican Volcanic Belt and implications for slab melting in hot and cold slab arcs. *Chem. Geol.* **377**, 45–55.

Caulfield J. T., Turner S. P., Smith I. E. M., Cooper L. B. and Jenner G. A. (2012) Magma Evolution in the Primitive, Intra-oceanic Tonga Arc: Petrogenesis of Basaltic Andesites at Tofua Volcano. *J. Petrol.* **53**, 1197–1230.

Chabaux F., Othman D. B. and Birck J. L. (1994) A new Ra-Ba chromatographic separation and its application to Ra mass-spectrometric measurement in volcanic rocks. *Chem. Geol.* **114**, 191 – 197.

Chauvel C., Marini J.-C., Plank T. and Ludden J. N. (2009) Hf-Nd input flux in the Izu-Mariana subduction zone and recycling of subducted material in the mantle. *Geochem. Geophys. Geosystems* **10**, n/a–n/a.

Chen Y. J. (1992) Oceanic crustal thickness versus spreading rate. *Geophys. Res. Lett.* **19**, 753–756.

Chiaradia M. (2009) Adakite-like magmas from fractional crystallization and melting-assimilation of mafic lower crust (Eocene Macuchi arc, Western Cordillera, Ecuador). *Chem. Geol.* **265**, 468 – 487.

Class C., Miller D. M., Goldstein S. L. and Langmuir C. H. (2000) Distinguishing melt and fluid subduction components in Umnak Volcanics, Aleutian Arc. *Geochem Geophys Geosyst* **1**, 1–30.

Coakley K. J., Simons D. S. and Leifer A. M. (2005) Secondary ion mass spectrometry measurements of isotopic ratios: correction for time varying count rate. *Int. J. Mass Spectrom.* **240**, 107–120.

Condomines M., Hemond C. and Allègre C. J. (1988) U-Th-Ra radioactive disequilibria and magmatic processes. *Earth Planet. Sci. Lett.* **90**, 243 – 262.

Cooper L. B., Plank T., Arculus R. J., Hauri E. H., Hall P. S. and Parman S. W. (2010) High-Ca boninites from the active Tonga Arc. *J. Geophys. Res. Solid Earth* **115**, n/a–n/a.

Cunningham H., Gill J., Turner S., Caulfield J., Edwards L. and Day S. (2012) Rapid magmatic processes accompany arc–continent collision: the Western Bismarck arc, Papua New Guinea. *Contrib. Mineral. Petrol.*, 1–16.

Defant M. J. and Drummond M. S. (1990) Derivation of some modern arc magmas by melting of young subducted lithosphere. *Nature* **347**, 662–665.

Dimalanta C., Taira A., Jr G. P. Y., Tokuyama H. and Mochizuki K. (2002) New rates of western Pacific island arc magmatism from seismic and gravity data. *Earth Planet. Sci. Lett.* **202**, 105 – 115.

Dreyer B. M., Morris J. D. and Gill J. B. (2010) Incorporation of Subducted Slab-derived Sediment and Fluid in Arc Magmas: B–Be–10Be–εNd Systematics of the Kurile Convergent Margin, Russia. *J. Petrol.* **51**, 1761–1782.

Dunk R. M., Mills R. A. and Jenkins W. J. (2002) A reevaluation of the oceanic uranium budget for the Holocene. *Chem. Geol.* **190**, 45 – 67.

Elliott T., Plank T., Zindler A., White W. and Bourdon B. (1997) Element transport from slab to volcanic front at the Mariana arc. *J Geophys Res* **102**, 14991–15019.

Freymuth H., Vils F., Willbold M., Taylor R. N. and Elliott T. (2015) Molybdenum mobility and isotopic fractionation during subduction at the Mariana arc. *Earth Planet. Sci. Lett.* **432**, 176–186.

Fukuda S., Nakai S. 'ichi, Niihori K., Tsukui M., Nakada S., Fujii T. and Tani K. (2008) 238U-230Th radioactive disequilibrium in the northern Izu arc: (230Th/232Th) in the sub-arc mantle. *Geochem. J.* **42**, 461–479.

Furukawa Y. and Tatsumi Y. (1999) Melting of a subducting slab and production of high-mg andesite magmas: Unusual magmatism in SW Japan at 13-15 Ma. *Geophys. Res. Lett.* **26**, 2271–2274.

Garrison J. M. and Davidson J. P. (2003) Dubious case for slab melting in the Northern volcanic zone of the Andes. *Geology* **31**, 565–568.

Gill J. B. (1981) *Orogenic Andesites and Plate Tectonics*., Springer-Verlag, Berlin.

Gill J. B., Morris J. D. and Johnson R. W. (1993) Timescale for producing the geochemical signature of island arc magmas: U-Th-Po and Be-B systematics in recent Papua New Guinea lavas. *Geochim. Cosmochim. Acta* **57**, 4269 – 4283.

Gill J. B. and Williams R. W. (1990) Th isotope and U-series studies of subduction-related volcanic rocks. *Geochim. Cosmochim. Acta* **54**, 1427–1442.

Gómez-Tuena A., Langmuir C. H., Goldstein S. L., Straub S. M. and Ortega-Gutiérrez F. (2007) Geochemical Evidence for Slab Melting in the Trans-Mexican Volcanic Belt. *J. Petrol.* **48**, 537–562.

Gotan K. (2008) Development of Be isotope analysis in volcanic rocks and its application to geochemical studies : Be isotopic constraints on the origin of U series disequilibria in the

volcanic rocks from Izu arc. University of Tokyo.

Green D. T. H. and Ringwood A. E. (1968) Genesis of the calc-alkaline igneous rock suite. *Contrib. Mineral. Petrol.* **18**, 105–162.

Hart S. R. and Staudigel H. (1982) The control of alkalies and uranium in seawater by ocean crust alteration. *Earth Planet. Sci. Lett.* **58**, 202–212.

Hawkesworth C. J., Turner S. P., McDermott F., Peate D. W. and van Calsteren P. (1997) U-Th Isotopes in Arc Magmas: Implications for Element Transfer from the Subducted Crust. *Science* **276**, 551–555.

Hochstaedter A. G., Gill J. B., Taylor B., Ishizuka O., Yuasa M. and Monta S. (2000) Across-arc geochemical trends in the Izu-Bonin arc: Constraints on source composition and mantle melting. *J Geophys Res* **105**, 495–512.

Hochstaedter A., Gill J., Peters R., Broughton P., Holden P. and Taylor B. (2001) Across-arc geochemical trends in the Izu-Bonin arc: Contributions from the subducting slab. *Geochem Geophys Geosyst* **2**, –.

Hoffmann D. L., Prytulak J., Richards D. A., Elliott T., Coath C. D., Smart P. L. and Scholz D. (2007) Procedures for accurate U and Th isotope measurements by high precision MC-ICPMS. *Int. J. Mass Spectrom.* **264**, 97–109.

Hoffmann D. L., Richards D. A., Elliott T. R., Smart P. L., Coath C. D. and Hawkesworth C. J. (2005) Characterisation of secondary electron multiplier nonlinearity using MC-ICPMS. *Int. J. Mass Spectrom.* **244**, 97–108.

Horwitz E. P., Chiarizia R., Dietz M. L., Diamond H. and Nelson D. M. (1993) Separation and preconcentration of actinides from acidic media by extraction chromatography. *Anal. Chim. Acta* **281**, 361–372.

Ishizuka O., Geshi N., Itoh J. 'ichi, Kawanabe Y. and TuZino T. (2008) The magmatic plumbing of the submarine Hachijo NW volcanic chain, Hachijojima, Japan: Long-distance magma transport? *J Geophys Res* **113**, B08S08–.

Ishizuka O., Taylor R. N., Milton J. A. and Nesbitt R. W. (2003) Fluid–mantle interaction in an intra-oceanic arc: constraints from high-precision Pb isotopes. *Earth Planet. Sci. Lett.* **211**, 221–236.

Jenner F. E. and O'Neill H. S. C. (2012) Analysis of 60 elements in 616 ocean floor basaltic glasses. *Geochem Geophys Geosyst* **13**, Q02005–.

Johnson M. C. and Plank T. (1999) Dehydration and melting experiments constrain the fate of subducted sediments. *Geochem. Geophys. Geosystems* **1**, n/a–n/a.

Karl S. M., Wandless G. A. and Karpoff A.-M. (1992) Sedimentological and geochemical characteristics of Leg 129 siliceous deposits eds. R. L. Larson, Y. Lancelot, A. Fisher, L. Abrams, R. Behl, W. H. Busch, G. Cameron, P. R. Castillo, J. M. Covington, G. Duerr, E. Erba, P. A. Floyd, C. France-Lanord, E. H. Hauser, S. M. Karl, A.-M. Karpoff, A. Matsuoka, A. Molinie, J. G. Ogg, A. R. M. Salimullah, M. Steiner, B. P. Wallick, W. Wightman, L. H. Dearmont, and N. K. McQuistion. *Proc. Ocean Drill. Program Sci. Results Old Pac. Crust Cover. Leg 129 Cruises Drill. Vessel JOIDES Resolut. Apra Harb. Guam Apra Harb. Guam Sites 800-802 20 Novemb. 1989-18 January 1990* **129**, 31–76.

Kay R. W. (1978) Aleutian magnesian andesites: Melts from subducted Pacific ocean crust. *J. Volcanol. Geotherm. Res.* **4**, 117 – 132.

van Keken P. E., Hacker B. R., Syracuse E. M. and Abers G. A. (2011) Subduction factory: 4. Depth-dependent flux of H2O from subducting slabs worldwide. *J Geophys Res* **116**, B01401–.

Kelemen P. B., Rilling J. L., Parmentier E. M., Mehl L. and Hacker B. R. (2003) Thermal structure due to solid-state flow in the mantle wedge beneath arcs. In *Geophys. Monogr. Ser.* AGU, Washington, DC. pp. 293–311. Available at: http://dx.doi.org/10.1029/138GM13.

Kelley K. A., Plank T., Ludden J. and Staudigel H. (2003) Composition of altered oceanic crust at ODP Sites 801 and 1149. *Geochem Geophys Geosyst* **4**, 8910–.

Kimura J.-I., Gill J. B., Kunikiyo T., Osaka I., Shimoshioiri Y., Katakuse M., Kakubuchi S., Nagao T., Furuyama K., Kamei A., Kawabata H., Nakajima J., van Keken P. E. and Stern R. J. (2014) Diverse magmatic effects of subducting a hot slab in SW Japan: Results from forward modeling. *Geochem. Geophys. Geosystems*, n/a–n/a.

Kimura J.-I., Kent A. J. R., Rowe M. C., Katakuse M., Nakano F., Hacker B. R., van Keken P. E., Kawabata H. and Stern R. J. (2010) Origin of cross-chain geochemical variation in Quaternary lavas from the northern Izu arc: Using a quantitative mass balance approach to identify mantle sources and mantle wedge processes. *Geochem Geophys Geosyst* **11**, Q10011–.

König S. and Schuth S. (2011) Deep melting of old subducted oceanic crust recorded by superchondritic Nb/Ta in modern island arc lavas. *Earth Planet. Sci. Lett.* **301**, 265 – 274.

Koornneef J. M., Stracke A., Aciego S., Reubi O. and Bourdon B. (2010) A new method for U–Th–Pa–Ra separation and accurate measurement of 234U–230Th–231Pa–226Ra disequilibria in volcanic rocks by MC-ICPMS. *Chem. Geol.* **277**, 30 – 41.

Koyama M. and Hayakawa Y. (1996) Syn- and Post-caldera Eruptive History of Izu Oshima Volcano based on Tephra and Loess Stratigraphy. *J. Geogr. Chigaku Zasshi* **105**, 133–162.

Lancelot Y. P., Larson R., Fisher A., Abrams L., Behl R., Busch W. H., Cameron G., Castillo P. R., Covington J. M., Durr G., Erba E., Floyd P. A., France-Lanord C., Hauser E. H., Karl S. M., Karpoff A.-M., Matsuoka A., Molinie A., Ogg J. G., Salimullah A. R. M., Steiner M., Wallick B. P. and Wightman W. (1990) Site 802 eds. Y. P. Lancelot, R. L. Larson, A. Fisher, L. Abrams, R. Behl, W. H. Busch, G. Cameron, P. R. Castillo, J. M. Covington, G. Durr, E. Erba, P. A. Floyd, C. France-Lanord, E. H. Hauser, S. M. Karl, A.-M. Karpoff, A. Matsuoka, A. Molinie, J. G. Ogg, A. R. M. Salimullah, M. Steiner, B. P. Wallick, W. Wightman, and L. H. Dearmont. *Proc. Ocean Drill. Program Old Pac. Crust Cover. Leg 129 Cruises Drill. Vessel JOIDES Resolut. Apra Harb. Guam Apra Harb. Guam Sites 800-802 20 Novemb. 1989-18 January 1990* **129**, 171–243.

Lundstrom C. C. (2003) Uranium-series Disequilibria in Mid-ocean Ridge Basalts: Observations and Models of Basalt Genesis. *Rev. Mineral. Geochem.* **52**, 175–214.

MacDougall J. D. (1977) Uranium in marine basalts: Concentration, distribution and implications. *Earth Planet. Sci. Lett.* **35**, 65–70.

McDermott F. and Hawkesworth C. (1991) Th, Pb, and Sr isotope variations in young island arc volcanics and oceanic sediments. *Earth Planet. Sci. Lett.* **104**, 1 – 15.

McDonough W. F. and Sun S. s. (1995) The composition of the Earth. *Chem. Evol. Mantle* **120**, 223–253.

Miyazaki T., Kimura J.-I., Senda R., Vaglarov B. S., Chang Q., Takahashi T., Hirahara Y., Hauff F., Hayasaka Y., Sano S., Shimoda G., Ishizuka O., Kawabata H., Hirano N., Machida S., Ishii T., Tani K. and Yoshida T. (2015) Missing western half of the Pacific Plate: Geochemical nature of the Izanagi-Pacific Ridge interaction with a stationary boundary between the Indian and Pacific mantles. *Geochem. Geophys. Geosystems* **16**, 3309–3332.

Morris J. D., Leeman W. P. and Tera F. (1990) The subducted component in island arc lavas: constraints from Be isotopes and B–Be systematics. *Publ. Online 01 March 1990 Doi101038344031a0* **344**, 31–36.

Münker C., Weyer S., Scherer E. and Mezger K. (2001) Separation of high field strength elements (Nb, Ta, Zr, Hf) and Lu from rock samples for MC-ICPMS measurements. *Geochem. Geophys. Geosystems* **2**, n/a–n/a.

Mutter A., Holzheid A., Klügel A., Wilke M., Berndt J. and Garbe-Schönberg D. (2014) Element signatures of subduction-zone fluids. An experimental study of the element partitioning (Dfluid/rock) of natural partly altered igneous rocks from the ODP drilling site 1,256. *Int. J. Earth Sci.* **103**, 1917–1927.

Newman S., Macdougall J. D. and Finkel R. C. (1984) 230Th-238U disequilibrium in island arcs: evidence from the Aleutians and the Marianas. *Nature* **308**, 268–270.

Nichols G. T., Wyllie P. J. and Stern C. R. (1994) Subduction zone melting of pelagic sediments constrained by melting experiments. *Nature* **371**, 785–788.

Patchett P. J. and Tatsumoto M. (1981) A routine high-precision method for Lu-Hf isotope geochemistry and chronology. *Contrib. Mineral. Petrol.* **75**, 263–267.

Peacock S. M. (2001) Are the lower planes of double seismic zones caused by serpentine dehydration in subducting oceanic mantle? *Geology* **29**, 299–302.

Peacock S. M., Rushmer T. and Thompson A. B. (1994) Partial melting of subducting oceanic crust. *Earth Planet. Sci. Lett.* **121**, 227 – 244.

Pearce J. A. (1982) Trace element characteristics of lavas from destructive plate boundaries. In *Andesites* John Willey, New York. pp. 525–548.

Pearce J. A., Kempton P. D., Nowell G. M. and Noble S. R. (1999) Hf-Nd Element and Isotope Perspective on the Nature and Provenance of Mantle and Subduction Components in Western Pacific Arc-Basin Systems. *J. Petrol.* **40**, 1579–1611.

Pin C. and Zalduegui J. S. (1997) Sequential separation of light rare-earth elements, thorium and uranium by miniaturized extraction chromatography: Application to isotopic analyses of silicate rocks. *Anal. Chim. Acta* **339**, 79 – 89.

Plank T., Kelley K. A., Murray R. W. and Stern L. Q. (2007) Chemical composition of sediments subducting at the Izu-Bonin trench. *Geochem Geophys Geosyst* **8**, Q04I16–.

Plank T. and Langmuir C. H. (1998) The chemical composition of subducting sediment and its consequences for the crust and mantle. *Chem. Geol.* **145**, 325–394.

Plank T. and Langmuir C. H. (1993) Tracing trace elements from sediment input to volcanic output at subduction zones. *Nature* **362**, 739–743.

Plank T., Ludden J. N., Escutia C. and al et (2000) Proceedings of the Ocean Drilling Program, Initial Reports vol. 185. *Ocean Drill Program Coll. Stn. Tex.*

Prytulak J., Elliott T., Hoffmann D. L. and Coath C. D. (2008) Assessment of USGS BCR-2 as a Reference Material for Silicate Rock U-Pa Disequilibrium Measurements. *Geostand. Geoanalytical Res.* **32**, 55–63.

Reagan M. K., Morris julie D., Herrstrom E. A. and Murrell M. T. (1994) Uranium series and beryllium isotope evidence for an extended history of subduction modification of the mantle below Nicaragua. *Geochim. Cosmochim. Acta* **58**, 4199–4212.

Regelous M., Collerson K. D., Ewart A. and Wendt J. I. (1997) Trace element transport rates in subduction zones: evidence from Th, Sr and Pb isotope data for Tonga-Kermadec arc lavas. *Earth Planet. Sci. Lett.* **150**, 291 – 302.

Rickli J., Frank M., Stichel T., Georg R. B., Vance D. and Halliday A. N. (2013) Controls on the incongruent release of hafnium during weathering of metamorphic and sedimentary catchments. *Geochim. Cosmochim. Acta* **101**, 263 – 284.

Savov I. P., Ryan J. G., D'Antonio M. and Fryer P. (2007) Shallow slab fluid release across and along the Mariana arc-basin system: Insights from geochemistry of serpentinized peridotites from the Mariana fore arc. *J. Geophys. Res. Solid Earth* **112**, B09205.

Savov I. P., Ryan J. G., D'Antonio M., Kelley K. and Mattie P. (2005) Geochemistry of serpentinized peridotites from the Mariana Forearc Conical Seamount, ODP Leg 125: Implications for the elemental recycling at subduction zones. *Geochem. Geophys. Geosystems* **6**, Q04J15.

Schmidt M. W. and Poli S. (1998) Experimentally based water budgets for dehydrating slabs and consequences for arc magma generation. *Earth Planet. Sci. Lett.* **163**, 361 – 379.

Schmidt M. W., Vielzeuf D. and Auzanneau E. (2004) Melting and dissolution of subducting crust at high pressures: the key role of white mica. *Earth Planet. Sci. Lett.* **228**, 65–84.

Scudder R. P., Murray R. W. and Plank T. (2009) Dispersed ash in deeply buried sediment from the northwest Pacific Ocean: An example from the Izu–Bonin arc (ODP Site 1149). *Earth Planet. Sci. Lett.* **284**, 639–848.

Spandler C., Pettke T. and Rubatto D. (2011) Internal and External Fluid Sources for Eclogite-facies Veins in the Monviso Meta-ophiolite, Western Alps: Implications for Fluid Flow in Subduction Zones. *J. Petrol.* **52**, 1207–1236.

Straub S. M., Goldstein S. L., Class C., Schmidt A. and Gomez-Tuena A. (2010) Slab and Mantle Controls on the Sr–Nd–Pb–Hf Isotope Evolution of the Post 42 Ma Izu–Bonin Volcanic Arc. *J. Petrol.* **51**, 993–1026.

Straub S. M., Zellmer G. F., Gómez-Tuena A., Espinasa-Pereña R., Martin-del Pozzo A. L., Stuart F. M. and Langmuir C. H. (2013) A genetic link between silicic slab components and calc-alkaline arc volcanism in central Mexico. *Geol. Soc. Lond. Spec. Publ.* **385**. Available at: http://sp.lyellcollection.org/content/early/2013/09/09/SP385.14.abstract.

Syracuse E. M., van Keken P. E. and Abers G. A. (2010) The global range of subduction zone thermal models. *Spec*. *Issue Deep Slab Mantle Dyn*. **183**, 73–90.

Tamura Y., Tani K., Chang Q., Shukuno H., Kawabata H., Ishizuka O. and Fiske R. S. (2007) Wet and Dry Basalt Magma Evolution at Torishima Volcano, Izu–Bonin Arc, Japan: the Possible Role of Phengite in the Downgoing Slab. *J*. *Petrol*. **48**, 1999–2031.

Tatsumi Y., Hamilton D. L. and Nesbitt R. W. (1986) Chemical characteristics of fluid phase released from a subducted lithosphere and origin of arc magmas: Evidence from high-pressure experiments and natural rocks. *J*. *Volcanol*. *Geotherm*. *Res*. **29**, 293 – 309.

Tatsumoto M. (1969) Lead isotopes in volcanic rocks and possible ocean-floor thrusting beneath island arcs. *Earth Planet*. *Sci*. *Lett*. **6**, 369 – 376.

Taylor R. N. and Nesbitt R. W. (1998) Isotopic characteristics of subduction fluids in an intra-oceanic setting, Izu–Bonin Arc, Japan. *Earth Planet*. *Sci*. *Lett*. **164**, 79 – 98.

Tera F., Brown L., Morris J., Sacks I. S., Klein J. and Middleton R. (1986) Sediment incorporation in island-arc magmas; inferences from $^{10\$}$Be. *Geochim*. *Cosmochim*. *Acta* **50**, 535–550.

Thompson A. B. (1992) Water in the Earth's upper mantle. *Nature* **358**, 295–302.

Tollstrup D., Gill J., Kent A., Prinkey D., Williams R., Tamura Y. and Ishizuka O. (2010) Across-arc geochemical trends in the Izu-Bonin arc: Contributions from the subducting slab, revisited. *Geochem Geophys Geosyst* **11**, Q01X10–.

Tollstrup D. L. and Gill J. B. (2005) Hafnium systematics of the Mariana arc: Evidence for sediment melt and residual phases. *Geology* **33**, 737–740.

Turner S., Bourdon B. and Gill J. (2003) Reviews in Mineralogy and Geochemistry, Volume 52: U-Series Geochemistry. In pp. 255–315.

Turner S., Hawkesworth C., Rogers N., Bartlett J., Worthington T., Hergt J., Pearce J. and Smith I. (1997) 238U/230Th disequilibria, magma petrogenesis, and flux rates beneath the depleted Tonga-Kermadec island arc. *Geochim*. *Cosmochim*. *Acta* **61**, 4855 – 4884.

Turner S., McDermott F., Hawkesworth C. and Kepezhinskas P. (1998) A U-series study of lavas from Kamchatka and the Aleutians: constraints on source composition and melting processes. *Contrib*. *Mineral*. *Petrol*. **133**, 217–234.

Ulmer P. and Trommsdorff V. (1995) Serpentine Stability to Mantle Depths and Subduction-Related Magmatism. *Science* **268**, 858–861.

Vance D. and Thirlwall M. (2002) An assessment of mass discrimination in MC-ICPMS using Nd isotopes. *Chem*. *Geol*. **185**, 227 – 240.

Wade J. A., Plank T., Stern R. J., Tollstrup D. L., Gill J. B., O'Leary J. C., Eiler J. M., Moore R. B., Woodhead J. D., Trusdell F., Fischer T. P. and Hilton D. R. (2005) The May 2003 eruption of Anatahan volcano, Mariana Islands: Geochemical evolution of a silicic island-arc volcano. *J*. *Volcanol*. *Geotherm*. *Res*. **146**, 139 – 170.

White W. M. and Dupré B. (1986) Sediment Subduction and Magma Genesis in the Lesser Antilles: Isotopic and Trace Element Constraints. *J Geophys Res* **91**, 5927–5941.

Woodhead J. D. (1989) Geochemistry of the Mariana arc (western Pacific): Source composition and processes. *Chem. Geol.* **76**, 1 – 24.

Woodhead J. D. and Fraser D. G. (1985) Pb, Sr and 10Be isotopic studies of volcanic rocks from the Northern Mariana Islands. Implications for magma genesis and crustal recycling in the Western Pacific. *Geochim. Cosmochim. Acta* **49**, 1925 – 1930.

Woodhead J. D., Harmon R. S. and Fraser D. G. (1987) O, S, Sr, and Pb isotope variations in volcanic rocks from the Northern Mariana Islands: implications for crustal recycling in intra-oceanic arcs. *Earth Planet. Sci. Lett.* **83**, 39–52.

Woodhead J. D., Hergt J. M., Davidson J. P. and Eggins S. M. (2001) Hafnium isotope evidence for "conservative" element mobility during subduction zone processes. *Earth Planet. Sci. Lett.* **192**, 331 – 346.

Woodhead J., Stern R. J., Pearce J., Hergt J. and Vervoort J. (2012) Hf-Nd isotope variation in Mariana Trough basalts: The importance of "ambient mantle" in the interpretation of subduction zone magmas. *Geology* **40**, 539–542.

Yogodzinski G. M., Brown S. T., Kelemen P. B., Vervoort J. D., Portnyagin M., Sims K. W. W., Hoernle K., Jicha B. R. and Werner R. (2015) The Role of Subducted Basalt in the Source of Island Arc Magmas: Evidence from Seafloor Lavas of the Western Aleutians. *J. Petrol.* **56**, 441–492.

Yogodzinski G. M., Lees J. M., Churikova T. G., Dorendorf F., Woerner G. and Volynets O. N. (2001) Geochemical evidence for the melting of subducting oceanic lithosphere at plate edges. *Nature* **409**, 500–504.

Yokoyama T., Kobayashi K., Kuritani T. and Nakamura E. (2003) Mantle metasomatism and rapid ascent of slab components beneath island arcs: Evidence from 238U-230Th-226Ra disequilibria of Miyakejima volcano, Izu arc, Japan. *J Geophys Res* **108**, 2329–2354.

Yokoyama T., Makishima A. and Nakamura E. (1999) Evaluation of the coprecipitation of incompatible trace elements with fluoride during silicate rock dissolution by acid digestion. *Chem. Geol.* **157**, 175 – 187.

Zellmer G. F., Iizuka Y., Miyoshi M., Tamura Y. and Tatsumi Y. (2012) Lower crustal H2O controls on the formation of adakitic melts. *Geology* **40**, 487–490.

Acknowledgments

HF was funded by a University of Bristol Postgraduate Research Scholarship and a short-term fellowship from the Japan Society for the Promotion of Science. NERC grant NE/H023933/1 covered some costs incurred during this study. Osamu Ishizuka, Yoshihisa Kawanabe, Akira Takada, and Kenji Niihori are thanked for sharing their samples from Hachijojima, Oshima, Aogashima, and Miyakejima, respectively. We thank Terry Plank for timely and high quality trace element analyses.

673 Table 1: Major element compositions of Izu arc lavas.

Island/sample	data source	SiO_2	TiO_2	AL_2O_3	Fe_2O_3	FeO T	CaO	MgO	MnO	K_2O	Na_2O	P2O5	latitude	longitude	rock type, petrography	Age
Oshima																
1986A-1	this study	52.12*	1.16	15.17	13.90		10.25	4.80	0.21	0.40	1.91	0.11	34°43'	139°23'	basaltic andesite, glassy, phenocryst-poor with minor plag	1986 eruption
S2-1	this study	51.36*	1.15	14.98	13.99		10.30	5.56	0.21	0.40	1.93	0.11	34°45'	139°23'	basalt, glassy, phenocryst-poor with minor plag	550 AD
N4-1	this study	52.18*	1.19	14.94	13.99		9.97	5.06	0.21	0.41	1.94	0.11	34°44'	139°22'	basaltic andesite, phenocryst-poor with minor plag	625 AD
Y5-1	this study	52.40*	1.23	14.27	14.65		9.78	4.87	0.22	0.43	2.04	0.11	34°45'	139°22'	basaltic andesite, phenocryst-poor with minor plag	1320 AD
Miyakejima																
1469	Fukuda et al. (2008)	53.55	1.29	15.01		12.86	9.24	4.55	0.24	0.56	2.55	0.15	34°05'	139°31'	basaltic andesite	1469 eruption
1874	Fukuda et al. (2008)	54.03	1.28	15.72		12.07	9.15	4.09	0.23	0.56	2.72	0.15	34°05'	139°31'	basaltic andesite	1874 eruption
1983-2903	Fukuda et al. (2008)	53.30	1.38	15.09		13.36	9.17	4.02	0.24	0.54	2.75	0.15	34°05'	139°31'	basaltic andesite	1983 eruption
MJ-12-02	this study	53.13*	1.28	15.19	13.49		9.24	3.91	0.22	0.55	2.83	0.15	34°05'	139°31'	basaltic andesite, glassy with plag and ol phenocrysts	1983 eruption
MJ-12-05	this study	49.60*	0.91	18.34	11.92		11.53	4.94	0.20	0.27	2.21	0.07	34°05'	139°31'	basalt, glassy with abundant plag phenocrysts, minor ol	
Hachichojima																
3102807	Ishizuka et al. (2008)	51.04	1.39	17.25		11.81	10.90	3.74	0.18	0.35	2.18	0.16	33°07'16"	139°48'58"	basalt	Holocene

3102804	Ishizuka et al. (2008)	52.41	1.60	14.66		13.77	9.08	4.07	0.21	0.44	2.36	0.19	33°07'23"	139°45'54"	basaltic andesite	Holocene
03102812A	Ishizuka et al. (2008)	50.57	1.31	18.10		11.36	11.23	3.62	0.17	0.33	2.13	0.14	33°06'40"	139°47'28"	basalt	Holocene
KT03-8 D16-1	Ishizuka et al. (2008)	50.86	1.34	17.43		11.82	10.90	3.96	0.18	0.35	2.08	0.15	33°10'52"	139°47'56"	basalt	Holocene
3103009	Ishizuka et al. (2008)	50.76	1.35	17.54		11.93	11.16	4.00	0.18	0.34	2.06	0.14	33°08'38"	139°45'22"	basalt	Holocene
Aogashima																
881105-2 lava	this study	58.83*	1.13	15.26	10.46		7.05	2.34	0.24	0.47	3.98	0.23	32°27'	139°46'	andesite, phenocryst-rich, dominantly plag	1781-1785 'Tenmai' eruption
T87071906	this study	53.05*	1.33	14.30	14.39		9.28	4.41	0.23	0.30	2.56	0.15	32°27'	139°46'	basaltic andesite, phenocryst-poor with minor ol and plag	>3 ka
Torishima																
1	Tamura et al. (2007)	51.80	0.65	20.59	9.92		11.68	3.38	0.15	0.29	2.22	0.08	30°29'	140°18'	basalt, plag-dominated cumulate	high Zr basalt from younger prehistoric unit (Tamura et al. 2007)
11	Tamura et al. (2007)	51.51	0.69	17.39	11.53		11.71	5.90	0.19	0.24	1.90	0.08	30°29'	140°18'	basalt with abundant plag + ol phenocrysts	high Zr basalt from younger prehistoric unit (Tamura et al. 2007)
24	Tamura et al. (2007)	54.66	0.79	17.02	11.66		9.62	4.08	0.20	0.30	2.66	0.18	30°29'	140°18'	basaltic andesite, glassy with plag + ol phenocrysts	high Zr basalt from 1939 eruption (Tamura et al. 2007)
37	Tamura et al. (2007)	54.49	0.78	17.16	11.63		9.50	4.04	0.20	0.30	2.61	0.17	30°29'	140°18'	basaltic andesite, glassy with plag phenocrysts	high Zr basalt from 1939 eruption (Tamura et al. 2007)
Niijima																
NJ-6A	Kimura et al. (2010)	49.61	1.11	16.79		13.07	9.95	5.43	0.20	0.33	2.23	0.12	30°20'	139°15'	basalt	>3 ka eruption from Wakago tuff ring
NJ-2	Kimura et al. (2010)	51.03	1.13	16.42		12.72	9.50	4.91	0.20	0.45	2.42	0.14	30°20'	139°15'	basalt	>3 ka eruption from Wakago tuff ring

NJ-1	Kimura et al. (2010)	51.29	1.11	16.62		12.69	9.48	5.03	0.20	0.49	2.35	0.13	30°20'	139°15'	basalt		>3 ka eruption from Wakago tuff ring

Ages for sampels from Oshima are from Koyama and Hayakawa (1996). *SiO_2 was calculated by difference to obtain a sum of major elements of 100 %.

Table 2: trace element compositions of Izu arc lavas. All concentrations are in µg/g.

Island/sample	Li	Be	Sc	Tl	V	Cr	Co	Ni	Cu	Zn	Ga	As	Rb	Sr	Y	Zr	Nb	Cs	Ba	La	Ce	Pr	Nd	Sm	Eu	Gd	Tb	Dy	Ho	Er	Tm	Yb	Lu	Hf	Ta	Pb	Th	U	data source
Oshima																																							
1986A-1	7.924	0.295	51.970	29.06	572.7	27.73	37.10	14.58	333.5	99.74	11.62	3.128	6.865	180.8	23.97	45.82	0.491	0.860	209.3	2.129	6.421	1.184	6.329	2.242	0.827	3.267	0.594	3.934	0.870	2.480		2.470	0.390	1.482	0.041	3.750	0.247	0.152	this study
S2-1	8.009	0.274	53.676	29.07	556.3	34.99	38.74	19.64	310.6	98.09	11.36	3.014	6.897	179.2	23.49	46.69	0.532	0.847	204.7	2.222	6.677	1.214	6.468	2.247	0.821	3.222	0.587	3.882	0.853	2.426		2.433	0.381	1.494	0.045	3.701	0.261	0.156	this study
N4-1	7.649	0.289	54.628	29.61	581.5	20.58	36.59	13.33	258.9	100.73	11.70	2.852	7.121	181.6	24.87	49.51	0.563	0.829	215.4	2.390	7.124	1.297	6.899	2.369	0.859	3.429	0.622	4.107	0.908	2.586		2.579	0.408	1.575	0.047	3.916	0.279	0.173	this study
Y5-1	8.682	0.313	55.679	110.32	625.1	20.44	38.63	15.79	244.7	106.27	11.87	10.118	7.333	176.7	25.39	49.79	0.550	0.857	225.7	2.348	6.994	1.290	6.905	2.414	0.880	3.530	0.640	4.267	0.939	2.673		2.670	0.422	1.609	0.046	4.154	0.276	0.168	this study
Miyakejima																																							
1469													7.900	239.0		66.40	0.600	0.600	207.0	3.710	10.800	1.790	9.440	3.160	1.150	4.270	0.760	5.070	1.080	3.320	0.480	3.240	0.480	2.210		3.430	0.335	0.192	Fukuda et al. (2008)
1874													7.720	244.0		66.30	0.640	0.580	206.0	3.660	10.900	1.800	9.600	3.280	1.150	4.300	0.750	5.240	1.130	3.400	0.490	3.330	0.500	2.300		3.430	0.324	0.193	Fukuda et al. (2008)
1983-2903													6.140	191.0		56.80	0.550		166.0	3.190	9.070	1.600	8.540	3.020	1.150	4.340	0.820	4.990	1.110	3.540	0.500	3.260	0.470	1.770		3.180	0.302	0.180	Fukuda et al. (2008)
1983-2903	7.866	0.526	46.605	42.38	462.5	6.63	32.42	8.39	165.4	114.27	11.88	2.373	8.013	247.9	31.68	69.87	0.658	0.572	199.4	3.360	9.962	1.835	9.712	3.299	1.190	4.551	0.819	5.242	1.139	3.227		3.199	0.505	2.159	0.058	3.327	0.324	0.193	this study
MJ-12-02	7.995	0.500	42.434	44.78	396.6	5.10	30.14	6.40	148.3	107.82	11.61	1.554	8.092	238.0	31.21	70.87	0.632	0.584	198.8	3.363	10.126	1.847	9.748	3.271	1.160	4.524	0.809	5.233	1.143	3.242		3.174	0.507	2.196	0.057	3.358	0.334	0.204	this study
MJ-12-05	4.864	0.320	42.967	11.47	392.7	36.72	32.33	14.50	125.0	105.22	9.25	0.631	3.200	255.4	18.68	35.50	0.287	0.114	111.3	1.590	4.943	0.951	5.120	1.823	0.777	2.619	0.475	3.144	0.682	1.950		1.924	0.304	1.123	0.028	1.618	0.123	0.083	this study
Hachichojima																																							
3102807													5.350	182.0	35.40	61.80	0.570	0.510	122.3	2.760	8.750	1.450	8.760	3.510	1.230	4.790	0.900	5.620	1.250	3.620	0.580	3.580	0.540	1.850	0.045	2.450	0.195	0.119	Ishizuka et al. (2008)
3102804													6.300	165.0	41.60	74.90	0.680	0.660	146.2	3.230	10.300	1.710	10.390	4.050	1.350	5.550	1.030	6.700	1.490	4.450	0.680	4.230	0.650	2.140	0.047	2.950	0.227	0.131	Ishizuka et al. (2008)
03102812A													4.770	188.0	34.50	61.50	0.530	0.480	120.6	2.550	8.110	1.360	8.370	3.120	1.120	4.230	0.810	5.370	1.150	3.390	0.530	3.300	0.480	1.760	0.047	2.480	0.180	0.111	Ishizuka et al. (2008)
KT03-8 D16-1													5.230	173.0	34.00	62.20	0.560	0.470	125.1	2.520	8.220	1.340	8.180	3.110	1.130	4.240	0.820	5.390	1.180	3.430	0.500	3.350	0.530	1.770	0.050	2.240	0.166	0.099	Ishizuka et al. (2008)
3103009													4.890	174.0	33.70	62.00	0.560	0.520	119.4	2.560	8.140	1.390	8.400	3.140	1.120	4.270	0.830	5.360	1.170	3.360	0.540	3.420	0.500	1.860	0.049	2.770	0.184	0.112	Ishizuka et al. (2008)
3103009	7.542	0.347	40.701	17.89	353.3	8.85	35.42	12.67	199.1	102.55	9.82	2.290	5.461	180.1	33.08	58.75	0.469	0.548	126.4	2.466	8.099	1.609	9.048	3.302	1.174	4.747	0.856	5.633	1.233	3.444		3.347	0.530	1.987	0.043	2.750	0.198	0.130	this study
Aogashima																																							
881105-2 lava	7.470	0.608	38.016	30.23	96.7	0.26	15.11	0.86	16.1	117.60	9.95	2.865	6.386	202.5	42.02	91.24	1.146	0.444	127.9	4.312	13.130	2.447	13.031	4.396	1.570	6.083	1.086	7.025	1.523	4.341		4.304	0.678	2.872	0.098	3.089	0.388	0.233	this study
T87071906	5.734	0.391	47.921	21.96	470.0	18.60	35.13	9.41	121.2	105.93	8.34	2.369	4.346	174.4	28.25	58.41	0.689	0.341	81.3	2.489	7.817	1.485	8.025	2.834	1.043	4.041	0.730	4.776	1.044	2.967		2.958	0.467	1.917	0.061	2.037	0.256	0.152	this study
Torishima																																							
1			30.300					11.90	132.0	65.20			3.120	190.4	16.20	32.30		0.085	66.9	1.710	4.860	0.878	4.820	1.750	0.664	2.480	0.441	3.010	0.666	2.000	0.296	1.980	0.302			2.240	0.170	0.145	Tamura et al. (2007)
11			43.200					22.40	163.7	74.90			3.170	159.0	16.20	30.80		0.280	60.8	1.650	4.670	0.846	4.750	1.750	0.660	2.510	0.457	3.130	0.693	2.040	0.302	1.970	0.311			1.710	0.162	0.135	Tamura et al. (2007)
24			37.700					10.50	165.0	94.80			3.590	177.0	20.90	36.10		0.327	72.8	2.040	5.910	1.080	6.180	2.280	0.864	3.230	0.583	3.890	0.864	2.580	0.381	2.510	0.391			2.530	0.172	0.147	Tamura et al. (2007)
24	7.149	0.283	38.354	33.90	335.3	3.82	32.67	9.79	172.3	85.33	7.94	1.951	4.303	186.7	23.52	40.36	0.383	0.360	72.6	1.938	5.884	1.162	6.376	2.260	0.861	3.285	0.589	3.886	0.860	2.447		2.459	0.391	1.376	0.035	2.605	0.165	0.141	this study
37			37.000					13.70	145.2	91.90			3.530	176.0	19.10	36.60		0.317	73.3	2.010	5.810	1.060	5.930	2.130	0.831	2.970	0.532	3.560	0.795	2.400	0.351	2.350	0.365			1.960	0.174	0.143	Tamura et al. (2007)
Niijima																																							
NJ-6A	5.970	0.360			400.0	24.52		11.04			17.22		5.790	270.4	17.10	66.70	1.035	0.309	99.7	3.863	9.610	1.480	7.341	2.248	0.871	2.906	0.454	3.099	0.653	1.777	0.281	1.899	0.284	1.213	0.065	3.850	0.493	0.169	Kimura et al. (2010)
NJ-2	5.127	0.517	45.539	55.72	391.6	9.30	33.72	6.92	72.3	89.69	9.09	0.704	7.485	277.1	20.50	54.42	1.342	0.391	98.6	3.768	10.380	1.680	8.293	2.485	0.967	3.191	0.553	3.539	0.760	2.136		2.096	0.329	1.495	0.102	2.491	0.474	0.195	this study
NJ-1	4.140	0.398			398.9	25.25		8.77			17.10		6.350	270.8	19.00	51.20	1.253	0.366	105.6	4.784	11.360	1.695	8.357	2.441	0.956	3.042	0.516	3.427	0.721	1.975	0.305	2.057	0.311	1.377	0.094	2.150	0.751	0.183	Kimura et al. (2010)
standards																																							
MAS1722	11.669	0.957	37.647	1.10	393.2	37.18	36.71	20.73	254.2	111.78	22.54	1.848	24.283	420.8	25.58	100.61	2.949	0.889	840.9	9.998	22.361	3.431	15.807	4.103	1.330	4.464	0.730	4.369	0.916	2.554	0.000	2.500	0.393	2.771	0.182	3.856	1.707	1.438	
MAR	5.629	0.403	39.300	1.23	261.0	321.00	53.40	150.90	73.7	78.40	15.00	0.627	0.933	91.9	31.70	79.10	1.433	0.026	6.5	2.027	6.980	1.340	7.373	2.790	1.023	4.140	0.757	5.110	1.130	3.240	0.000	3.183	0.494	2.170	0.234	0.312	0.093	0.067	

K1919	4.950	1.100	30.300	2.70	304.0	245.00	49.30	98.00	145.0	98.00	21.00	0.947	10.352	398.0	26.90	186.00	20.054	0.095	135.0	15.056	38.528	5.583	25.115	6.195	2.074	6.408	1.004	5.483	1.018	2.568	0.000	2.065	0.298	4.772	1.400	1.096	1.234	0.420
W-2	9.700	0.740	35.000	1.06	262.0	93.00	44.00	70.00	111.0	77.00	17.30	1.240	22.000	197.0	21.90	93.10	7.700	0.902	171.6	10.070	22.790	3.040	12.900	3.240	1.100	3.730	0.632	3.830	0.800	2.170	0.000	1.980	0.300	2.480	0.500	7.700	2.100	0.490

Table 3: Radiogenic isotope compositions of Izu arc lavas. Errors are 2σ standard errors for samples and 2σ standard deviations for standards. N = number of analyses.

location	sample	$^{143}Nd/^{144}Nd$	2s	$^{87}Sr/^{86}Sr$	2s	$^{176}Hf/^{177}Hf$	2s
Oshima	1986A-1	0.513107	5.6E−06	0.703689	8.7E−06	0.283290	0.000014
	S2-1	0.513107	5.8E−06	0.703639	5.5E−06	0.283286	0.000006
	N4-1	0.513107	5.5E−06	0.703664	6.9E−06	0.283289	0.000006
Miyakejima	1469	0.513106	5.6E−06	0.703455	7.3E−06	0.283262	0.000006
	1874						
	1983-2903	0.513108	5.4E−06	0.703481	5.8E−06	0.283263	0.000006
	MJ-12-02	0.513105	5.1E−06	0.703444	5.2E−06	0.283261	0.000004
	MJ-12-05	0.513105	4.6E−06	0.703476	5.1E−06	0.283256	0.000005
Hachichojima	3102807						
	3102804	0.513102	5.4E−06	0.703566	6.2E−06	0.283234	0.000004
	03102812A	0.513101	4.9E−06	0.703531	6.5E−06	0.283236	0.000006
	3103009	0.513096	6.0E−06	0.703523	6.5E−06	0.283226	0.000005
Aogashima	881105-2 lava	0.513081	6.0E−06	0.703405	5.4E−06	0.283218	0.000005
	T87071906	0.513080	6.5E−06	0.703431	8.9E−06	0.283219	0.000006
Torishima	1	0.513118	4.9E−06	0.703472	5.4E−06	0.283277	0.000004
	11	0.513120	4.6E−06	0.703477	5.4E−06	0.283273	0.000005
	24	0.513111	5.3E−06	0.703464	8.7E−06	0.283272	0.000009
	37	0.513117	5.6E−06	0.703518	9.5E−06	0.283266	0.000008
Niijima	NJ-2	0.513068	5.0E−06	0.703336	5.8E−06	0.283229	0.000004

	NJ-1	0.513060	7.4E−06	0.703371	5.5E−06	0.283230	0.000005
standards	BCR-2	0.512636	2.1E-06 (n=4)	0.705007	2.2E-05 (n=4)	0.282869	5.0E-06 (n=4)
	BHVO-2	0.512985	1.6E-06 (n=2)	0.703468	1.2E-05 (n=2)	0.283099	2.2E-07 (n=2)
	JB-2	0.513106	3.7E-06 (n=4)	0.703672	2.6E-05 (n=5)	0.283252	3.0E-06 (n=4)

Table 4: U-Series data for Izu arc lavas. Samples with ($^{234}U/^{238}U$) > 1.005 are considered altered. Data for these samples are shown in italics and are not plotted in Fig. 8, 10 and 11. Errors are 2σ standard errors (SE) for samples and 2σ standard deviations (SD) for standards. N = number of analyses.

location	sample	U [ng/g]	± 2SE	($^{234}U/^{238}U$)	± 2SE	Th [ng/g]	± 2SE	($^{230}Th/^{232}Th$)	± 2SE	($^{238}U/^{230}Th$)	($^{238}U/^{232}Th$)	± 2SE	($^{230}Th/^{238}U$)	± 2SE	($^{226}Ra/^{230}Th$)	age (y BP)	($^{226}Ra/^{230}Th)_{initial}$	^{226}Ra [fg/g]
Oshima	1986A-1	151.7	0.2	1.0028	0.0027	249.8	0.5	1.256	0.0022	1.47	1.843	0.0031	0.682	0.002	2.060	27	2.073	72
	S2-1	154.6	0.1	1.0015	0.0025	261.9	1.0	1.247	0.0025	1.44	1.791	0.0067	0.696	0.003				
	N4-1	170.5	0.2	1.0008	0.0014	277.4	0.6	1.249	0.0070	1.49	1.866	0.0037	0.670	0.004	1.609	1390	2.112	62
	Y5-1	164.2	0.1	1.0026	0.0008	271.5	0.4	1.264	0.0024	1.45	1.836	0.0008	0.689	0.001				
Miyakejima	1469	196.5	0.1	1.0017	0.0015	343.4	1.4	1.376	0.0023	1.26	1.737	0.0065	0.792	0.003	2.496	544	2.894	131
	1874	196.7	0.1	1.0016	0.0009	334.8	1.2	1.394	0.0028	1.28	1.783	0.0057	0.782	0.003	2.808	139	2.920	146
	1983-2903	187.6	0.1	1.0015	0.0013	316.7	0.5	1.389	0.0019	1.29	1.798	0.0014	0.773	0.001	3.108	30	3.136	152
	MJ-12-02	199.9	0.2	1.0021	0.0016	331.5	2.6	1.411	0.0039	1.30	1.830	0.0142	0.771	0.006				
	MJ-12-05	*80.9*	*0.1*	*1.0071*	*0.0014*	*122.6*	*0.7*	*1.436*	*0.0030*	*1.39*	*2.002*	*0.0109*	*0.717*	*0.004*				
Hachichojima	3102807	130.6	0.1	1.0018	0.0018	205.4	1.1	1.471	0.0043	1.31	1.930	0.0098	0.762	0.005	1.937	holocene		65
	3102804	158.5	0.2	1.0014	0.0017	246.5	0.4	1.504	0.0039	1.30	1.951	0.0025	0.771	0.002				
	03102812A	121.2	0.1	1.0007	0.0007	191.6	0.9	1.464	0.0024	1.31	1.920	0.0084	0.763	0.004	2.129	holocene		66
	KT03-8 D16-1	133.4	0.2	1.0041	0.0012	202.9	0.3	1.479	0.0030	1.35	1.995	0.0034	0.741	0.002				
	3103009	124.2	0.1	1.0004	0.0012	194.5	0.7	1.463	0.0022	1.33	1.938	0.0061	0.755	0.003				
Aogashima	881105-2 lava	224.8	0.2	1.0009	0.0012	382.5	1.4	1.634	0.0035	1.09	1.784	0.0062	0.916	0.004	1.409	230	1.452	98
	T87071906	147.8	0.2	1.0010	0.0014	250.3	0.9	1.662	0.0048	1.08	1.791	0.0064	0.928	0.004	1.288	>3000	>2.056	60
Torishima	1	133.2	0.2	1.0044	0.0031	158.1	0.8	2.014	0.0062	1.27	2.555	0.0126	0.788	0.005				
	11	124.2	0.1	1.0043	0.0012	146.4	1.1	1.995	0.0058	1.29	2.573	0.0188	0.775	0.006				
	24	135.8	0.1	1.0045	0.0018	161.7	0.4	1.980	0.0073	1.29	2.548	0.0053	0.777	0.003	2.374	74	2.419	85
	37	130.0	0.1	1.0041	0.0011	157.9	0.2	2.027	0.0048	1.23	2.498	0.0027	0.811	0.002	2.291	74	2.333	82
Niijima	*NJ-6A*	*180.6*	*0.1*	*1.0190*	*0.0009*	*384.3*	*1.2*	*1.111*	*0.0039*	*1.28*	*1.426*	*0.0038*	*0.780*	*0.003*				
	NJ-2	187.7	0.1	1.0016	0.0011	466.7	2.2	1.099	0.0017	1.11	1.221	0.0054	0.900	0.004	2.087	ca. 3000		119
	NJ-1	191.8	0.1	1.0022	0.0019	510.1	0.8	1.119	0.0028	1.02	1.141	0.0011	0.981	0.003	1.881	ca. 3000		120
volcaniclastic sediments	800A-36R-03-28							0.539	0.0046									

	801B-5R-01W-40-42							0.656	0.0043						
	801B-7R-01W-35-37							0.384	0.0027						
	802A-16R-01-30-33							0.920	0.0063						
	802A_19R-2-67-72							0.817	0.0052						
	802A-40R-01W-87-89							0.462	0.0031						
	802A-43R-01W-57-59							0.447	0.0032						
	802A-47R-03W-52-54							0.874	0.0087						
standards	BCR-2 (n=5)	1703.1	18.9	1.0027	0.0011	5921.8	35.3	0.877	0.0012	0.873	0.0067	1.005	0.007		
	TML (n=1)	10326.4	17.7	1.0001	0.0006	29473.7	103.8	1.0798	0.0006	1.0631	0.004	1.016	0.004	1.033	
				($^{234}U/^{238}U$)	± 2SD			$^{230}Th/^{232}Th$	± 2SD						
	IRMM 036 (n=7)							3.060E−06	7.95067E−09						
	Harwell Uraninite (n=7)			0.9998	0.0010										

Table 5: Model parameters for U-Series and Hf-Nd isotope ratios in Izu arc lavas (Fig. 10)

	sediment [μg/g]	AOC [μg/g]	D solid/liquid (slab melt)	D solid/liquid (slab fluid)	MORB (subducted slab, Fig. 10a) [μg/g]	MORB (from Izu mantle, Fig 10c) [μg/g]
Th	4.39 (a)	0.173 (d)	0.1557 (g)	1.437 (h)	0.385 (i)	
U	0.92 (a)	0.390 (d)	0.167 (g)	0.187 (h)	0.121 (i)	
Nb	5.22 (a)	2.89 (d)	0.272 (g)			
Nd	25.2 (a)	11.3 (d)	0.662 (g)			4 (k)
Hf	1.44 (a)	3.07 (d)	1.923 (g)			1 (k)
(230Th/232Th)	0.65 (b)	7.0 (e)			0.98 (j)	
143Nd/144Nd	0.512336 (c)	0.51314 (f)				0.51312 / 0.51317
176Hf/177Hf	0.282897 (c)	0.28320 (f)				0.283235 / 0.283295

(a) average sediment from ODP Site 1149 (Plank et al., 2007)

(b) average sediment from ODP Site 1149 (Plank et al., 2007) assuming secular equilibrium

(c) bulk composition of ODP Site 1149 sediment (Chauvel et al., 2009)

(d) AOC super composite from ODP Site 801 (Kelley et al., 2003)

(e) AOC super composite from ODP Site 801 (Kelley et al., 2003) assuming secular equilibrium

(f) average of ODP Site 1149 AOC from Miyazaki et al. (2015)

(g) 4 GPa, 900 °C partition coefficients from Kessel et al. (2005)

(h) 4 GPa fluid partition coefficients from Turner et al. (2003)

(i) average MORB from Jenner and O'Neill (2012)

(j) average MORB from Jenner and O’Neill (2012) assuming secular equilibrium

(k) Nd and Hf concentrations within the lower end of concentrations in MORB (Jenner and O'Neill, 2012) were chosen to represent melt derived from a depleted sub-arc mantle

Table 6: Izu arc Th and ^{10}Be input and ouput fluxes

Input

	Th [µg/g]	Th subduction rate (kg x year^{-1} x km)	^{10}Be	^{10}Be subduction rate (atoms x year^{-1} x km^{-1})
sediments (400 m thickness)	4.39 (a)	275.3	1.4x10^{13} atoms x cm^{-2} (b)	1.84x10^{18} (c)
AOC (800 m thickness)	0.173 (d)	29.48	-	-

Output

	Th [µg/g]	Th output rate (kg x year^{-1} x km^{-1})	^{10}Be	^{10}Be output rate (atoms x year^{-1} x km^{-1})
primitive Izu arc lavas	0.123 (e)	22.39	440000 atoms x g^{-1} (f)	8.01x10^{16} (f)
- derived from sediments	-	20.77-17.46 (g)	440000 atoms x g^{-1} (f)	8.01x10^{16} (f)
- derived from AOC	-	1.61-4.93 (g)	-	-

Subduction parameters

subduction angle	46	degrees (h)
slab top distance	117	km (h)
subduction rate	5.6	cm x year^{-1} (i)
oceanic crustal thickness	6	km (j)
density sediments, AOC, arc magma	2.8	g x cm^{-3}
arc magma production rate	65	km^3 x km^{-1} x Ma^{-1} (k)

(a) Plank et al. (2007)

(b) Dreyer et al. (2010)

(c) ^{10}Be corrected for decay during sediment transport to depth beneath the volcanic front

(d) Kelley et al. (2003) using data for ODP Site 801 instead of ODP Site 1149 due to the larger thickness of AOC sampled, see text for details

(e) [Th] in least differentiated sample (MJ-12-05), assuming primary composition, see Table 1,2

(f) ^{10}Be content in Izu arc lavas from Gotan (2008), assuming the lowest ^{10}Be concentration represents the primary magma

(g) the fraction of Th output from sediments and AOC is derived from Th isotope ratios using average (^{230}Th/^{232}Th) of sediments from ODP Site 1149 and AOC from ODP Site 801, , respectively (Fig. 11) and the range in (^{230}Th/^{232}Th) in Izu arc lavas (1.10-2.03, Table 4)

(h) Syracuse et al. (2010)

(i) Bird (2003)

(j) Chen (1992)

(k) Dimalanta et al. (2002)

Figure

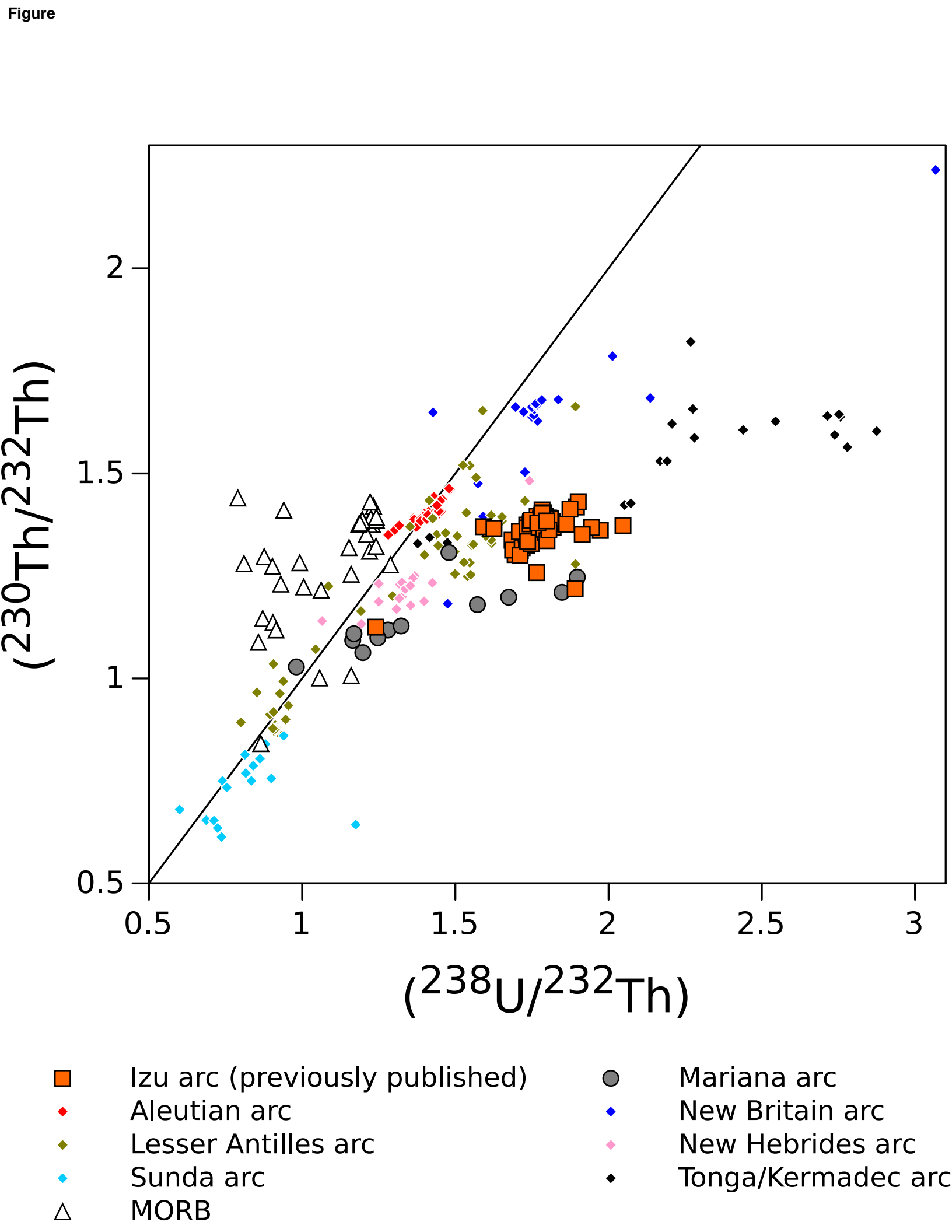
2
1.5
1
0.5
0.5
1
1.5
2
2.5
3
$(^{230}Th/^{232}Th)$
$(^{238}U/^{232}Th)$
Izu arc (previously published)
Aleutian arc
Lesser Antilles arc
Sunda arc
MORB
Mariana arc
New Britain arc
New Hebrides arc
Tonga/Kermadec arc

Figure

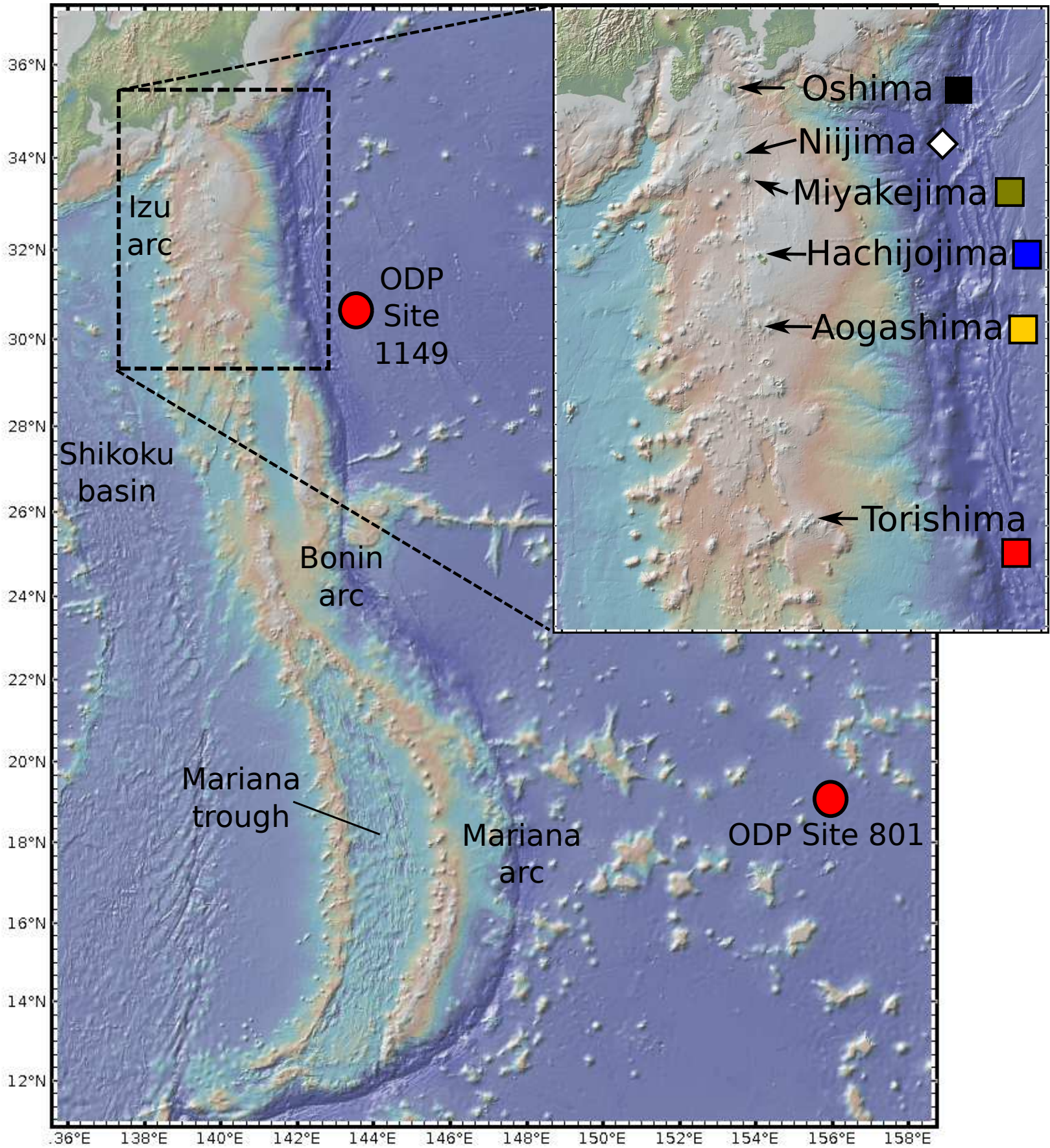
Oshima
Niijima
Miyakejima
Hachijojima
Aogashima
Torishima
Izu
arc
ODP
Site
1149
Shikoku
basin
Bonin
arc
Mariana
trough
Mariana
arc
ODP Site 801
36°N
34°N
32°N
30°N
28°N
26°N
24°N
22°N
20°N
18°N
16°N
14°N
12°N
136°E
138°E
140°E
142°E
144°E
146°E
148°E
150°E
152°E
154°E
156°E
158°E

Figure

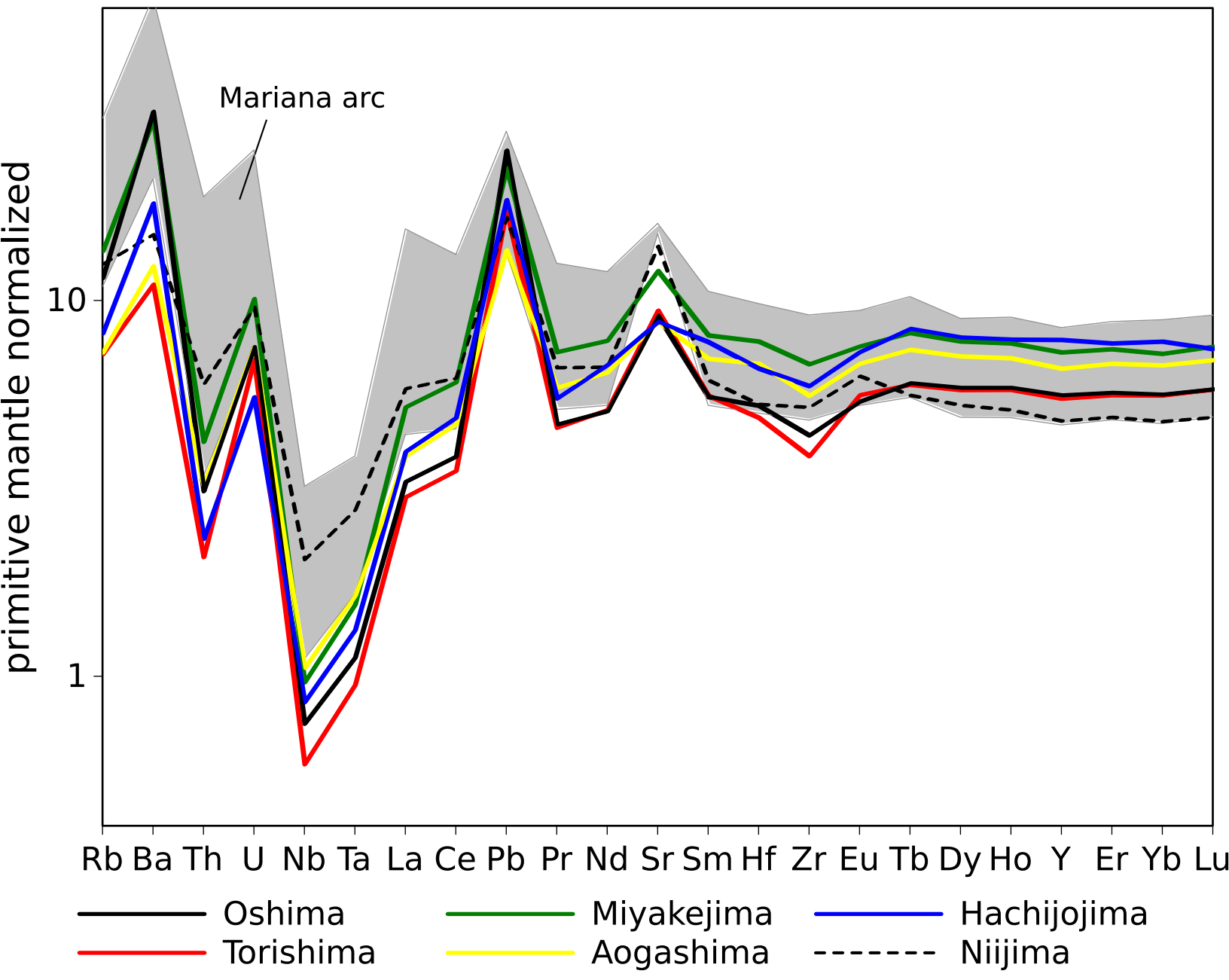
Mariana arc
primitive mantle normalized
10
1
Rb Ba Th U Nb Ta La Ce Pb Pr Nd Sr Sm Hf Zr Eu Tb Dy Ho Y Er Yb Lu
Oshima
Torishima
Miyakejima
Aogashima
Hachijojima
Niijima

Figure

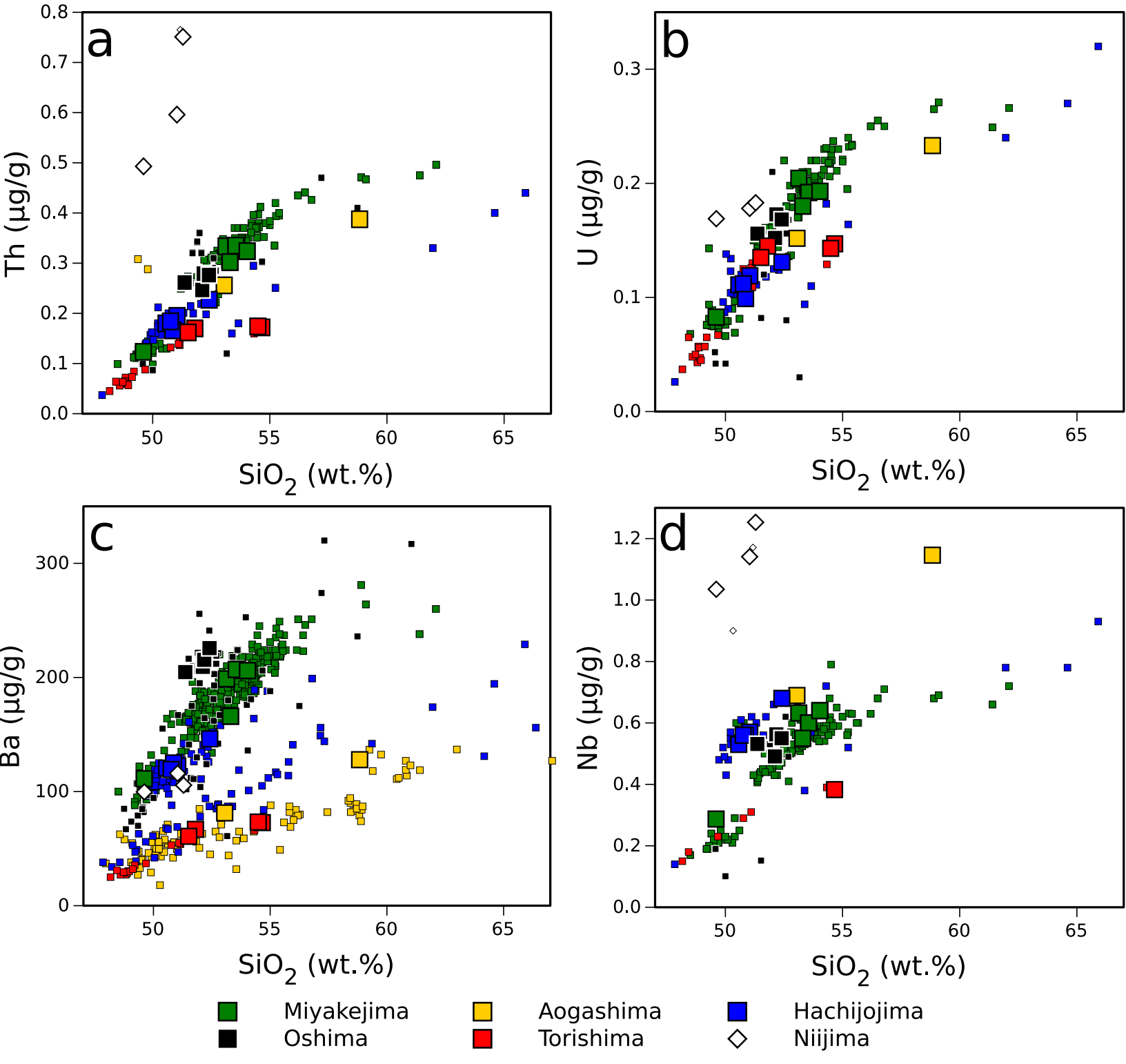
a
b
c
d
Th (µg/g)
U (µg/g)
Ba (µg/g)
Nb (µg/g)
SiO2 (wt.%)
Miyakejima
Oshima
Aogashima
Torishima
Hachijojima
Niijima

Figure

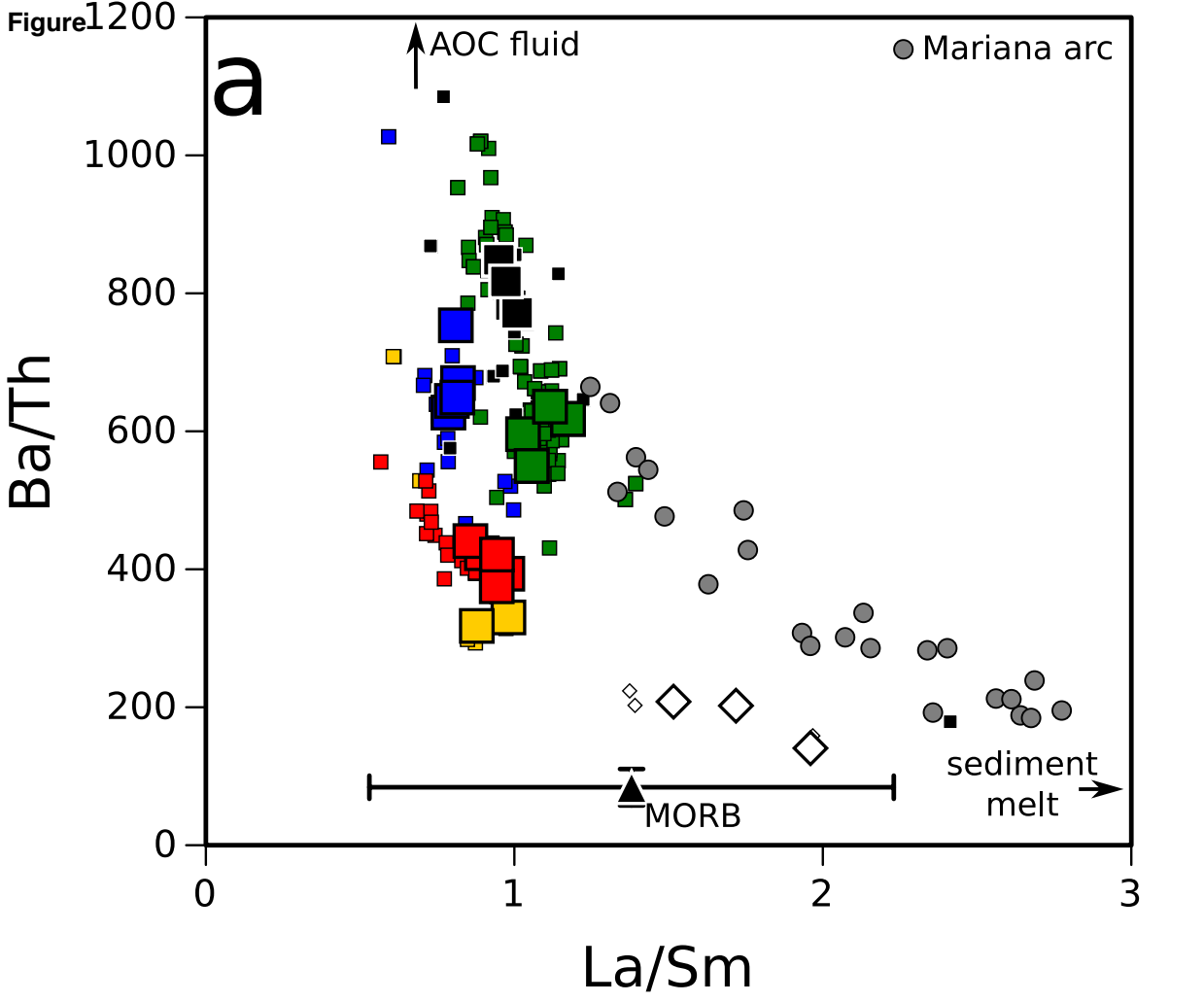
a
AOC fluid
Mariana arc
1200
1000
800
600
400
200
0
Ba/Th
0
1
2
3
La/Sm
MORB
sediment
melt

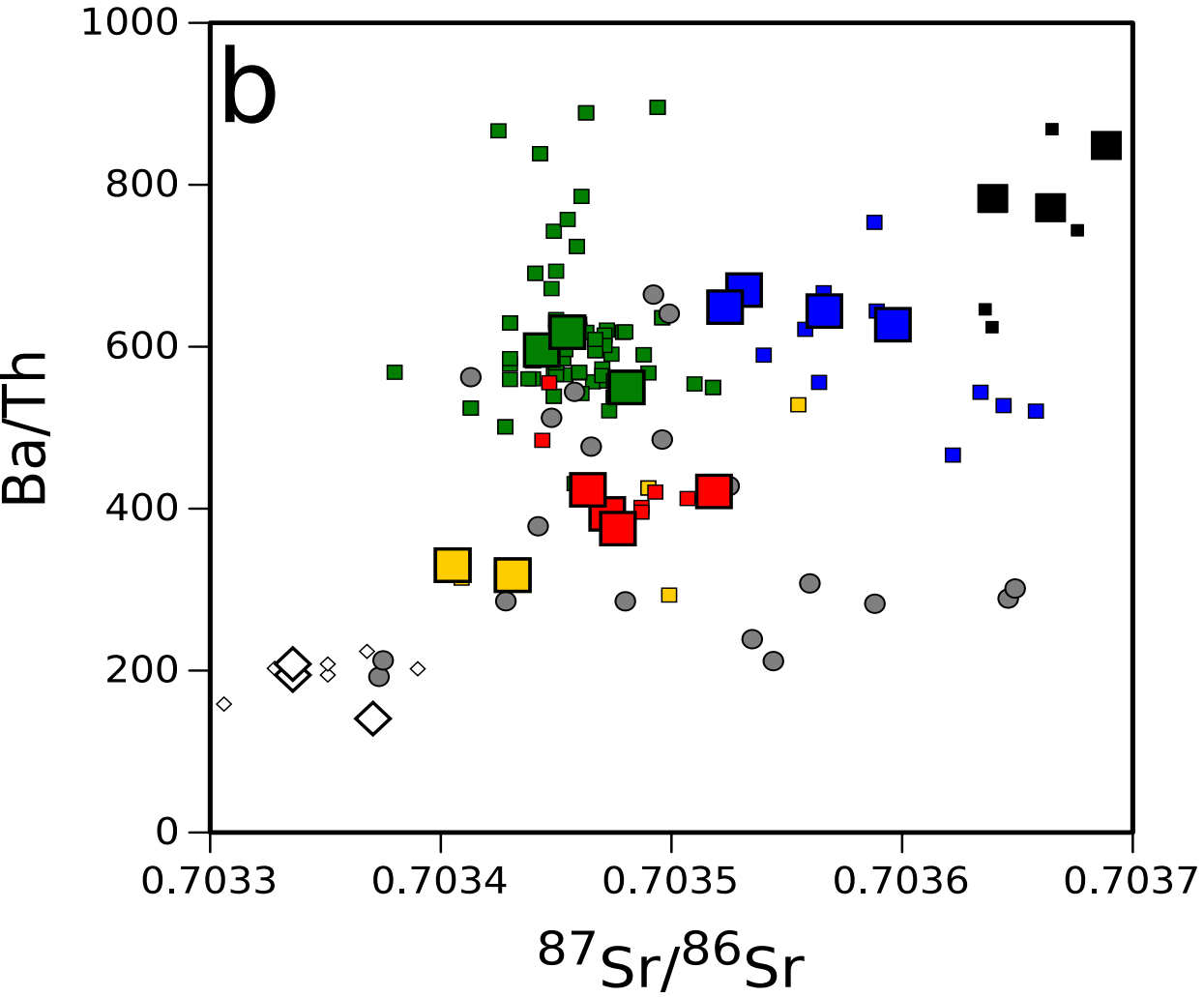
b
1000
800
600
400
200
0
Ba/Th
0.7033
0.7034
0.7035
0.7036
0.7037
87Sr/86Sr

Figure

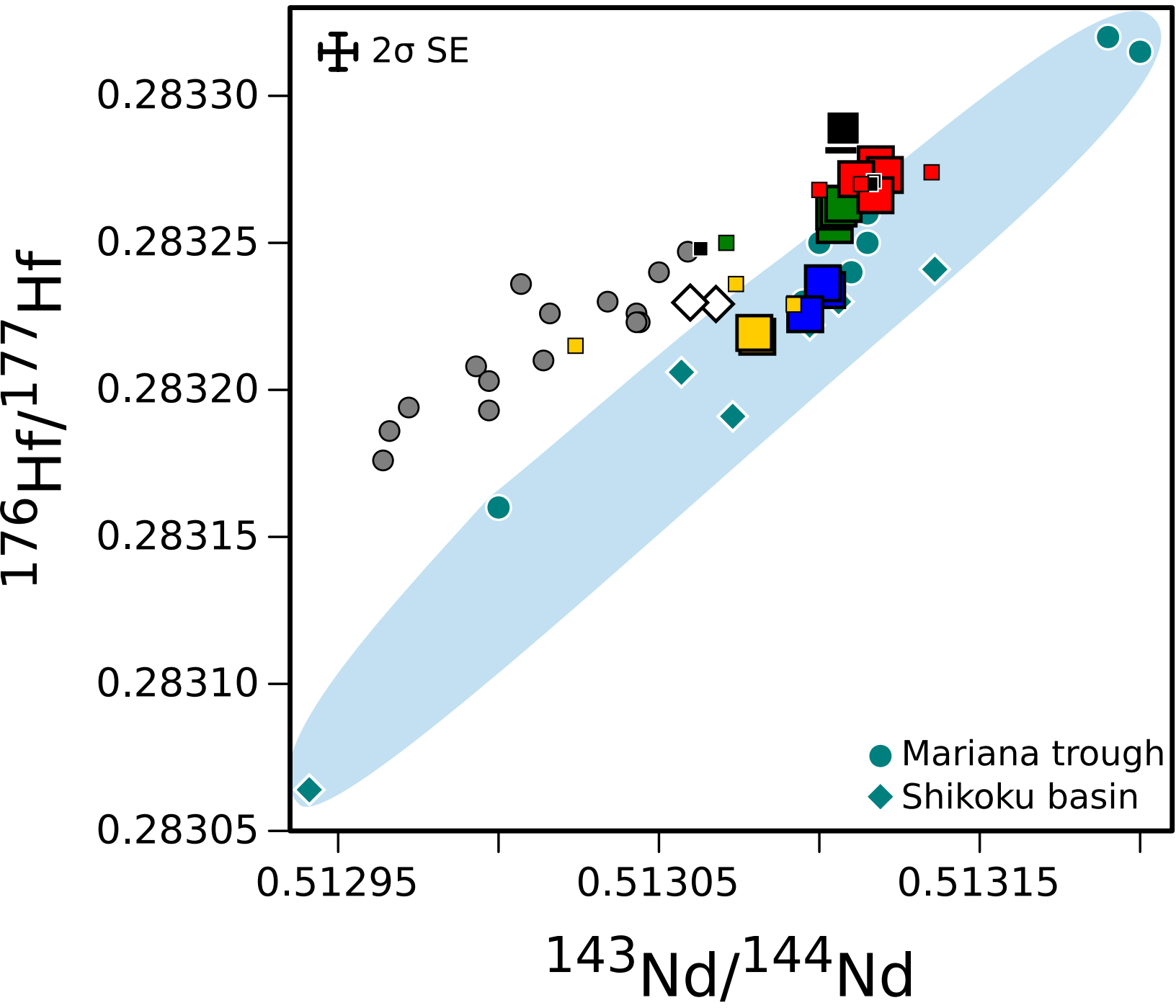
2σ SE
0.28330
0.28325
0.28320
0.28315
0.28310
0.28305
176Hf/177Hf
0.51295
0.51305
0.51315
143Nd/144Nd
Mariana trough
Shikoku basin

Figure

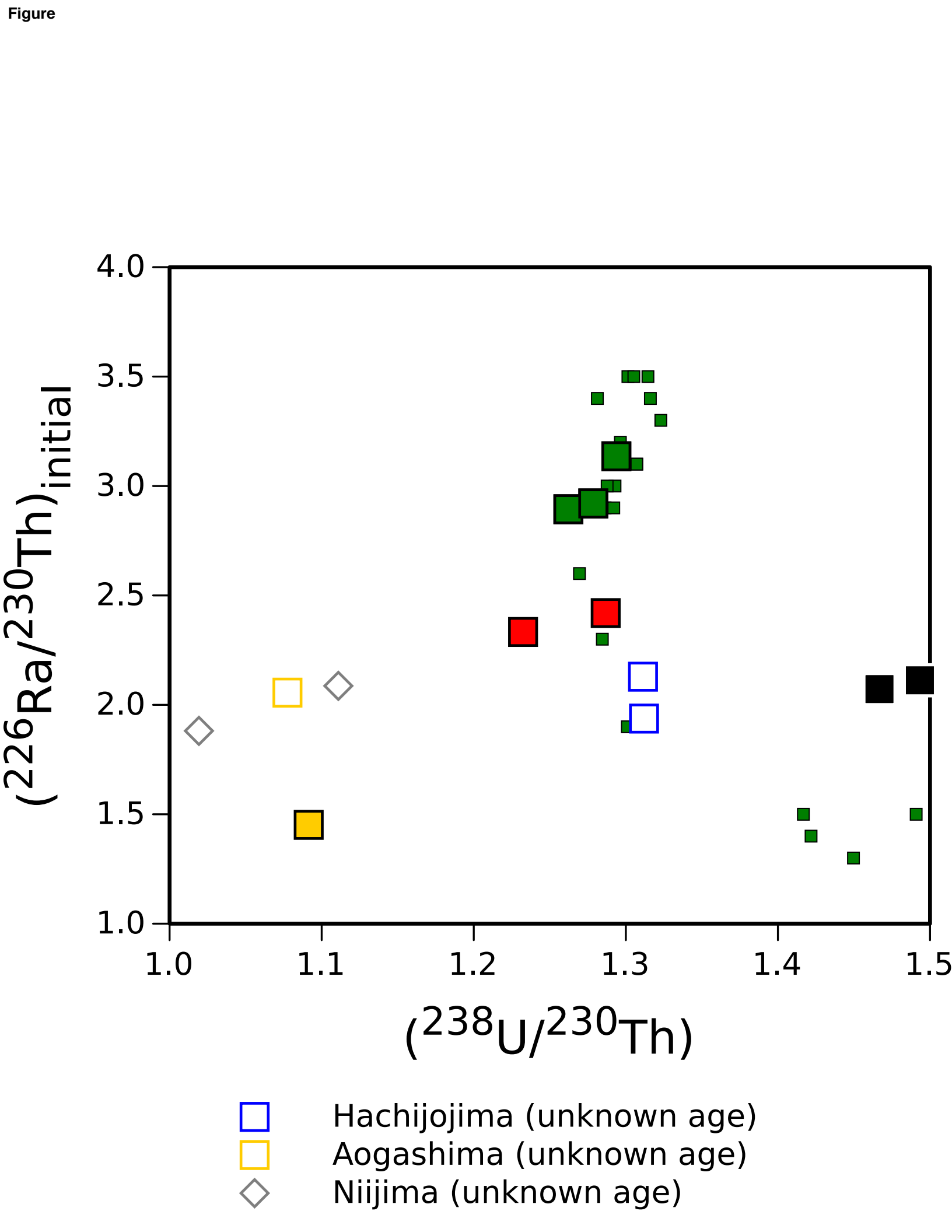
4.0
3.5
3.0
2.5
2.0
1.5
1.0
1.0
1.1
1.2
1.3
1.4
1.5
$(^{226}Ra/^{230}Th)_{initial}$
$(^{238}U/^{230}Th)$
Hachijojima (unknown age)
Aogashima (unknown age)
Niijima (unknown age)

Figure

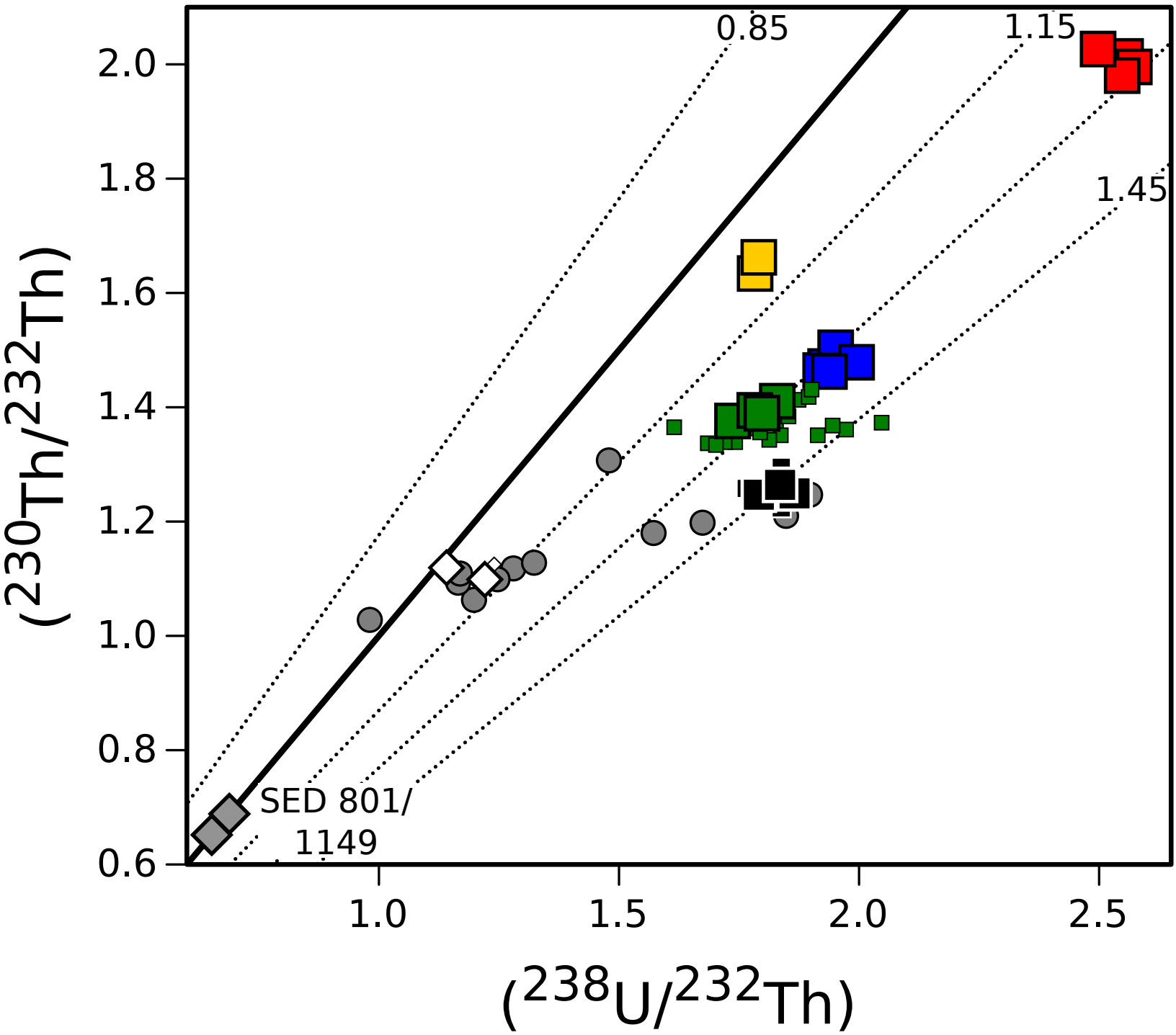
0.85
1.15
1.45
SED 801/
1149
2.0
1.8
1.6
1.4
1.2
1.0
0.8
0.6
1.0
1.5
2.0
2.5
(230Th/232Th)
(238U/232Th)

Figure

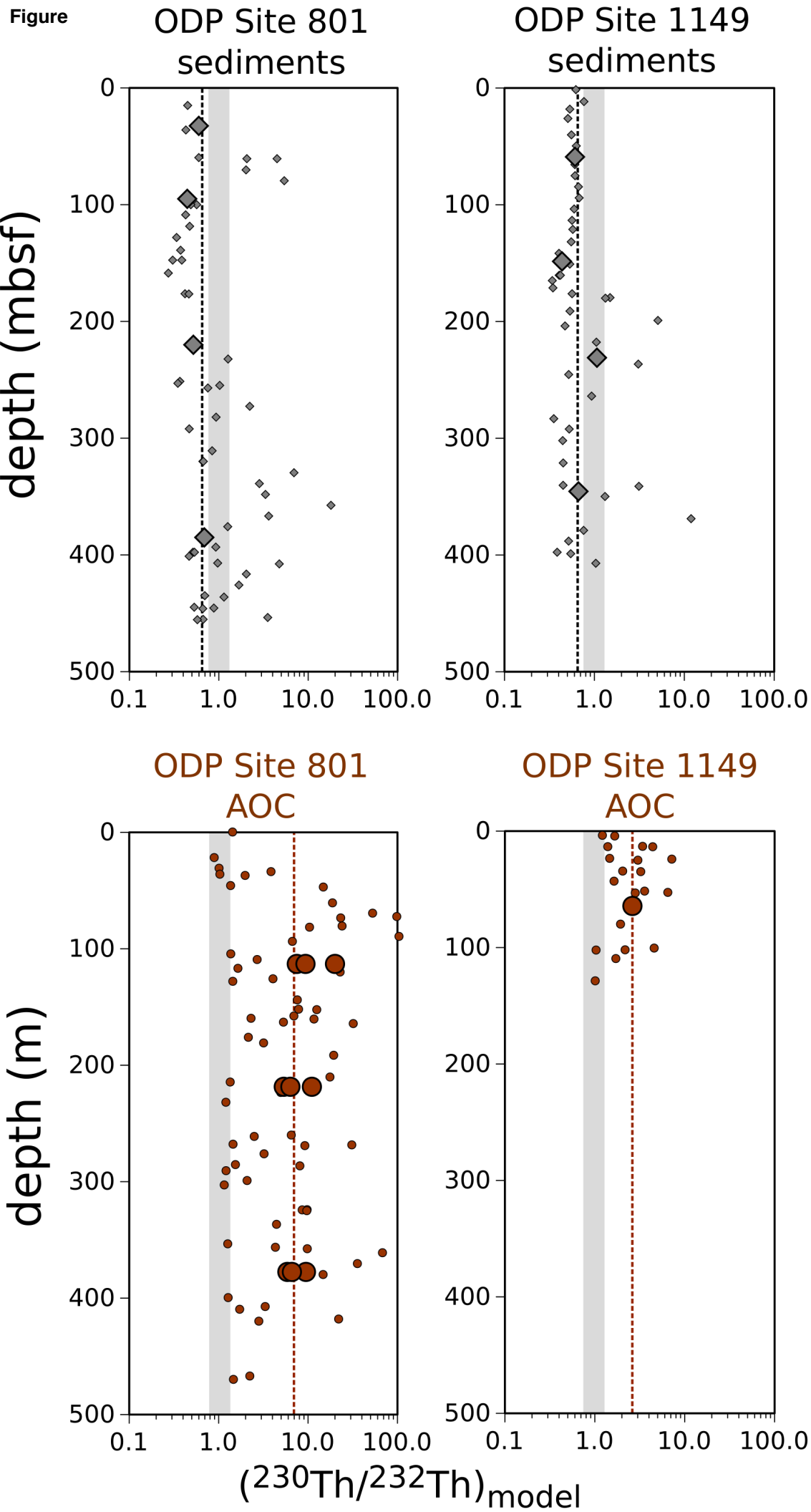
ODP Site 801
sediments
ODP Site 1149
sediments
ODP Site 801
AOC
ODP Site 1149
AOC
depth (mbsf)
depth (m)
0
100
200
300
400
500
0.1
1.0
10.0
100.0
(230Th/232Th)model

Figure

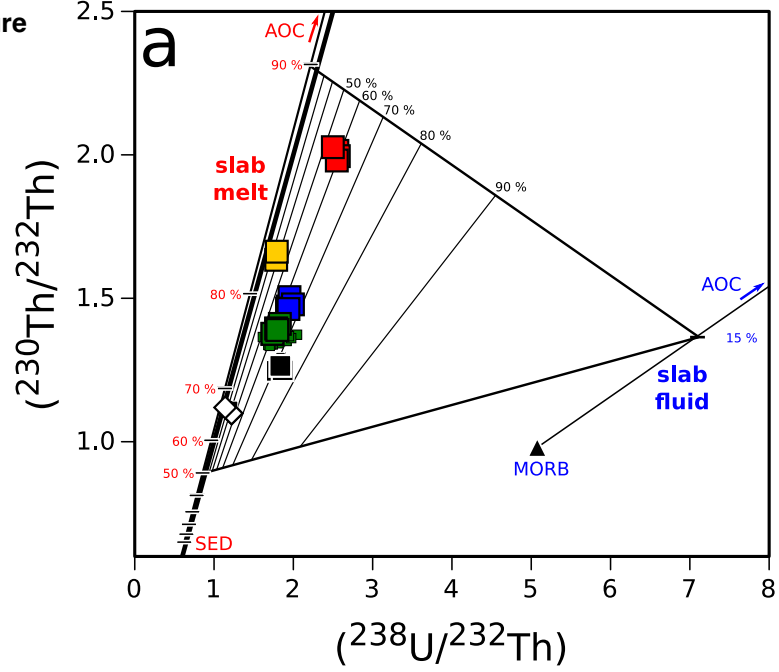
a
AOC
90 %
50 %
60 %
70 %
80 %
90 %
slab
melt
80 %
70 %
60 %
50 %
SED
AOC
15 %
slab
fluid
MORB
2.5
2.0
1.5
1.0
0
1
2
3
4
5
6
7
8
(230Th/232Th)
(238U/232Th)

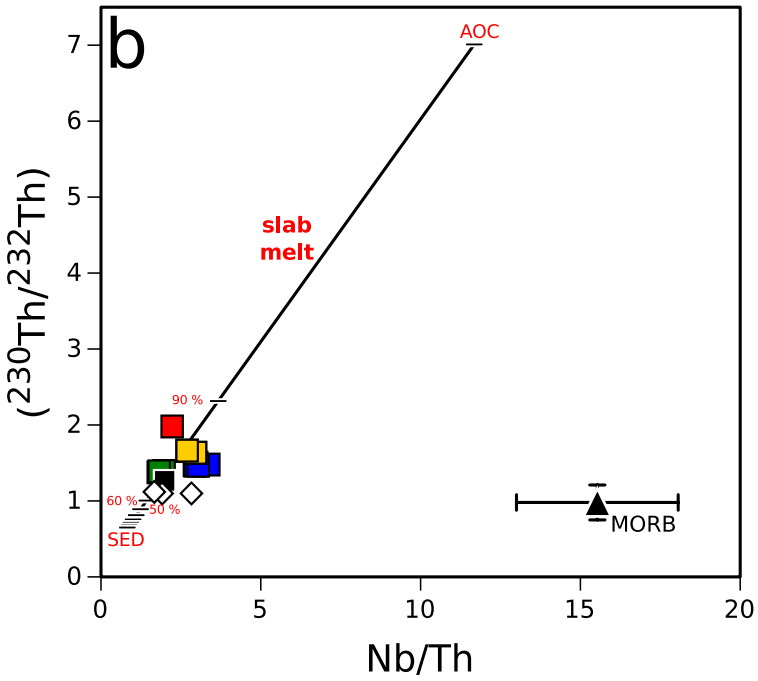
b
AOC
slab
melt
90 %
60 %
50 %
SED
MORB
7
6
5
4
3
2
1
0
0
5
10
15
20
(230Th/232Th)
Nb/Th

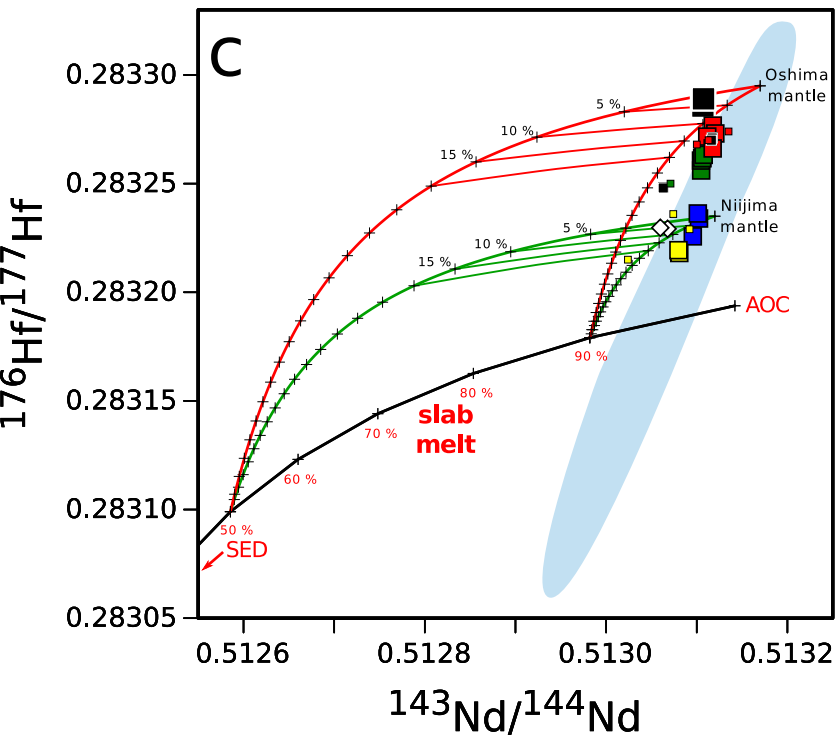
c
Oshima
mantle
5 %
10 %
15 %
Niijima
mantle
5 %
10 %
15 %
AOC
90 %
80 %
70 %
slab
melt
60 %
50 %
SED
0.28330
0.28325
0.28320
0.28315
0.28310
0.28305
0.5126
0.5128
0.5130
0.5132
176Hf/177Hf
143Nd/144Nd

Figure

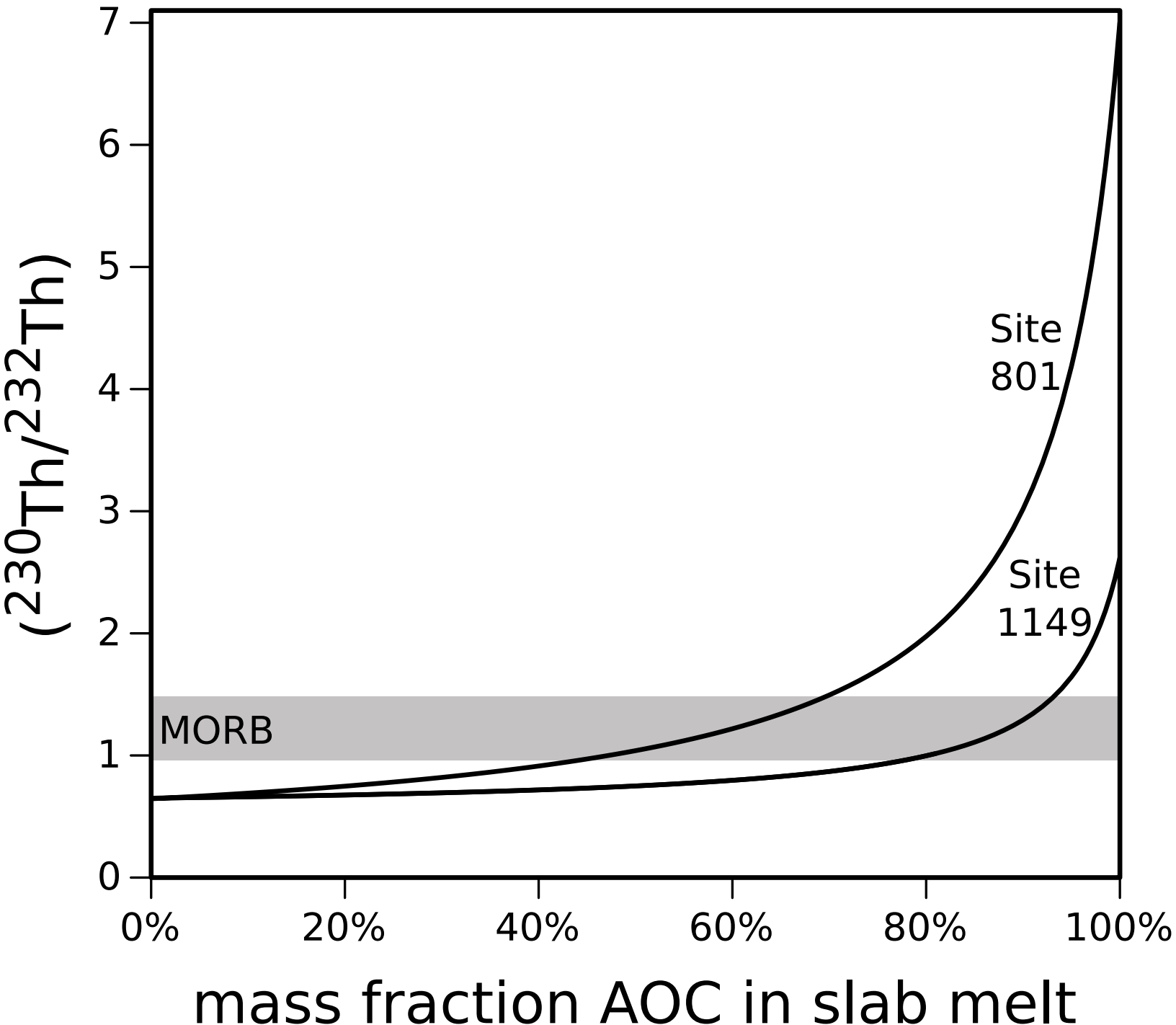
7
6
5
4
3
2
1
0
(230Th/232Th)
Site
801
Site
1149
MORB
0%
20%
40%
60%
80%
100%
mass fraction AOC in slab melt